Itaconate controls the severity of pulmonary fibrosis

Patricia P. Ogger[1], Gesa J. Albers[1,2], Richard J. Hewitt[1,3], Brendan J. O'Sullivan[4,5], Joseph E. Powell[6,7], Emily Calamita[1], Poonam Ghai[1], Simone A. Walker[1], Peter McErlean[1], Peter Saunders[3], Shaun Kingston[3], Philip L. Molyneaux[1,3], John M. Halket[8], Robert Gray[8], Daniel C. Chambers[4], Toby M. Maher[1,3], Clare M. Lloyd[1,2], Adam J. Byrne[1,2*]

*Corresponding author

[1]National Heart & Lung Institute,
Imperial College London,
SW7 2AZ, UK

[2]Asthma UK Centre in Allergic Mechanisms of Asthma,
London, UK

[3]Royal Brompton Hospital, Sydney Street, London,
SW3 6NP, UK

[4]Queensland Lung Transplant Service,
The Prince Charles Hospital,
Brisbane,
Queensland,
Australia

[5]Faculty of Medicine,

The University of
Queensland,
Brisbane,
Queensland,
Australia

[6]Garvan-Weizmann Centre for Cellular Genomics,
Garvan Institute of Medical Research,
Darlinghurst, Sydney,
Australia

[7]Cellular Genomics Futures Institute,
University of New South Wales,
Kensington,
Sydney,
Australia

[8]Mass Spectrometry Facility
King's College London,
SE1 9NH, UK

Keywords: idiopathic pulmonary fibrosis, airway macrophage, metabolism, itaconate, aconitate decarboxylase.

Abstract

Idiopathic pulmonary fibrosis (IPF) is a fatal lung disease where airway macrophages (AMs) play a key role. Itaconate has emerged as a mediator of macrophage function, but its role during fibrosis is unknown. Here, we reveal that itaconate is an endogenous anti-fibrotic factor in the lung. Itaconate levels are reduced in bronchoalveolar lavage and itaconate-synthesizing cis-aconitate decarboxylase expression (*ACOD1)* is reduced in AMs from IPF patients compared to controls. In the murine bleomycin model of pulmonary fibrosis, *Acod1*$^{-/-}$ mice unlike WT littermates, develop persistent fibrosis. Pro-fibrotic gene expression is increased in *Acod1*$^{-/-}$ tissue-resident AMs compared to WT and adoptive transfer of WT-monocyte-recruited AMs rescued disease phenotype. Culture of lung fibroblasts with itaconate decreased proliferation and wound healing capacity and inhaled itaconate was protective in mice, *in vivo*. Collectively, these data identify itaconate as critical for controlling the severity of lung fibrosis and targeting this pathway may be a viable therapeutic strategy.

Introduction

Idiopathic pulmonary fibrosis (IPF) is a chronic debilitating lung disease, characterized by the deposition of excessive extracellular matrix in the lung parenchyma (Martinez et al., 2017). Existing pharmacological options are limited and with an increasing worldwide incidence and a median survival of 3 years from diagnosis, there is an urgent requirement to understand pathological mechanisms involved (Hutchinson et al., 2015; Kreuter et al., 2015). A growing body of evidence supports a role for airway macrophages (AMs) in regulating pathogenic mechanisms underlying IPF (Allden et al., 2019). AMs are crucial in contributing to pulmonary defense, repair, surfactant processing and inflammatory responses (Byrne et al.,

2015). Moreover, AMs are strategically positioned at the interface between the airways and the environment and are found in the alveoli and airways, secreting numerous pro-fibrotic soluble mediators, chemokines, and matrix metalloproteases (Hussell and Bell, 2014). Macrophages demonstrate remarkable plasticity and are capable of acquiring phenotypes which can both drive or resolve fibro-proliferative responses to injury (Murray et al., 2014; Wynn and Vannella, 2016). For example, AMs have been shown to be involved in the regulation of the extracellular matrix via secretion of matrix metalloproteases (MMPs) or by direct uptake of collagen (Atabai et al., 2009; Dancer et al., 2011). We have recently related AM phenotype to disease outcome in IPF, since increased numbers of AMs lacking the transferrin receptor CD71 are associated with worsened disease (Allden et al., 2019).

Macrophage activation is tightly linked to cellular metabolism (O'Neill et al., 2016). Inflammatory activation of macrophages results in impaired mitochondrial respiration and tricarboxylic acid (TCA) cycle disruption, resulting in the accumulation of endogenous metabolites capable of adopting immunomodulatory roles (Mills et al., 2016). One such bioactive metabolite is itaconate. In macrophages, synthesis of itaconate is catalyzed by cis-aconitate decarboxylase (CAD), encoded by aconitate decarboxylase 1 (*ACOD1*), which mediates the decarboxylation of cis-aconitate to itaconate (Domínguez-Andrés et al., 2019; Michelucci et al., 2013). Itaconate is one of the most highly induced metabolites in activated bone marrow derived macrophages (BMDMs, Basler et al., 2006; Cordes et al., 2016; Lee et al., 1995; Strelko et al., 2011) and can suppress the expression of pro-inflammatory cytokines (Lampropoulou et al., 2016). Furthermore, itaconate has been shown to control macrophage effector functions *via* competitive inhibition of succinate dehydrogenase (SDH) mediated oxidation of succinate and furthermore, drives an anti-inflammatory

program via the KEAP-1-NRF2 axis (Lampropoulou et al., 2016; Mills et al., 2018). Therefore, itaconate appears to be a crucial regulator of macrophage phenotype and function. However, its functional significance in specialized tissue resident macrophages during chronic respiratory disease such as IPF remains unknown.

Here, we show that the ACOD1/itaconate axis is altered in the human lung during IPF, itaconate is an anti-fibrotic factor in the murine lung and it impairs human fibroblast activity. In patients with IPF, there is decreased expression of *ACOD1* in AMs and reduced levels of airway itaconate, compared to healthy controls. Acod1 deficiency in mice leads to more severe disease pathology, which is further exacerbated by adoptive transfer of *Acod1*$^{-/-}$, but not WT monocyte-recruited AMs. Addition of exogenous itaconate to cultures of human lung fibroblasts limits proliferation and wound healing and furthermore, inhaled itaconate ameliorates lung fibrosis in mice. Together, our data indicate that the *ACOD1*/itaconate axis is an endogenous pulmonary regulatory pathway, which limits fibrosis. Our data therefore highlight itaconate and cis-aconitate decarboxylase as potential therapeutic targets in IPF and other chronic respiratory diseases where fibrosis plays a role.

Results

ACOD1/itaconate pathway is altered during IPF

In order to determine the distribution of *ACOD1* mRNA in the human lung, we assessed expression levels in primary AMs, lung fibroblasts (HLF) and human bronchial epithelial cells (HBEs) from healthy volunteers and IPF patients. AMs were enriched using magnetic associated cell sorting (MACS) based on CD206 expression, as this marker has been identified as most expressed on human airway macrophages

(Bharat et al., 2016) (Supplementary Table 1-2 for patient demographics). *ACOD1* was expressed in $CD206^{+}$ AMs from healthy volunteers and this expression level was significantly reduced in cells from IPF, when assessed by qPCR (**Figure 1A** and **supplementary Figure 1A, 1B**). Furthermore, levels of BAL itaconate (normalized to total protein) were decreased in IPF patients compared to healthy controls (**Figure 1B**). In contrast, we could not detect any *ACOD1* transcript in HLFs or HBE's (*data not shown*). These results indicate that the *ACOD1*/itaconate axis is significantly altered in the lungs of individuals with fibrotic lung disease.

Acod1 deficiency results in worsened pulmonary fibrosis in mice

To mechanistically assess the role of *Acod1*/itaconate in the pathogenesis of pulmonary fibrosis, we next utilized the murine bleomycin model of pulmonary fibrosis. Wild-type (WT) mice were instilled with a single dose of bleomycin via the oropharyngeal route (**Figure 1C**) and expression of *Acod1* in lungs assessed at inflammatory (d7), peak fibrosis (d21) and late (d42) phases of the disease. Compared to PBS controls, *Acod1* expression was significantly elevated at d7 and d21 post bleomycin, returning to baseline levels at d42. *Acod1* reached maximum-expression levels at d21 post bleomycin, corresponding with both inflammation and peak fibrosis (**Figure 1D**). Furthermore, itaconate levels in BAL were assessed by targeted gas chromatography–mass spectrometry (GC-MS) at these different time points. Compared to PBS controls, itaconate was significantly increased at d7 and d21 post bleomycin and returned to baseline levels at d42 (**Figure 1E**). In order to determine whether *Acod1* played a role in the establishment or severity of fibrosis, we assessed the response of *Acod1*-deficient mice to bleomycin. Although WT mice showed improved fibrosis, pathology and lung function, $Acod1^{-/-}$ mice failed to return to baseline levels at d42 and had increased BAL cell counts (**Figure 1H**). In order to

149 determine the impact of *Acod1*-deficiency on immune responses in the lung we
150 performed multi-parameter flow cytometry using a gating strategy shown in
151 **Supplementary Figure 2A**. Although total numbers of AMs are much higher post
152 bleomycin than numbers of neutrophils, both were elevated in *Acod1*$^{-/-}$ compared to
153 WT mice at d42 (**Figure 1F and G**). Furthermore, *Acod1*$^{-/-}$ had worsened airway
154 resistance, elastance and compliance compared to WT controls at day 42 post
155 bleomycin exposure (**Figure 1I**). However, in comparison to WT controls, *Acod1*-
156 deficient mice did not show altered lung function (**Supplementary Figure 3A and C**),
157 total BAL counts (**Supplementary Figure 3B and D**) or pathology (**Supplementary**
158 **Figure 4C**) at d7 or d21 post-injury, suggesting that itaconate does not play a role in
159 the initiation of fibrosis. Total AM numbers (**Supplementary Figure 3E**) were not
160 altered when comparing WT and *Acod1*$^{-/-}$ mice at d7 or d21 post challenge. We saw a
161 reduction in neutrophil numbers, comparing WT and *Acod1*$^{-/-}$ mice, at day 7 post
162 challenge, but no alteration at d21 (**Supplementary Figure 3F**). Adaptive immunity
163 did not appear to be altered in *Acod1*$^{-/-}$ mice compared to WT controls, with no
164 alteration in T- or NK-cells at any time-point (**Supplementary Figure 3G and H**).
165 *Acod1*$^{-/-}$ mice showed increased expression of *Collagen-(Col)3α1* and *Fibronectin-1*
166 (*Fn-1*) (**Figure 2A**), compared to WT controls at day 21, but not at d7/42
167 (**Supplementary Figure 4A and B**). We did not observe any statistically significant
168 change in lung expression of *Col1α1* or *Col4α1* at any time point assessed in this
169 model (**Figure 2A and supplementary Figure 4A - B**). Ashcroft scoring of Sirius red
170 stained lung slices indicated that pathology did not change in *Acod1*$^{-/-}$ mice at day 21
171 post bleomycin compared to WT (**Supplementary Figure 4C**). *Acod1*$^{-/-}$ mice had
172 enhanced pulmonary fibrosis compared to WT controls, characterized by increased
173 lung hydroxyproline levels (**Figure 2B**) and Ashcroft scores (**Figure 2C** and **D**).

Consistent with these findings, *Acod1*$^{-/-}$ mice showed increased levels of superoxide in in the CD45^{+} compartment of whole lung tissue in comparison to WT (**Figure 2E, Supplementary Figure 2B**), further suggesting more severe disease in *Acod1*$^{-/-}$. Furthermore, no change in lung function parameters, BAL cell count, AMs or neutrophils was detected at baseline (in PBS mice) in WT compared to *Acod1*$^{-/-}$ mice (**Supplementary Figure 5**). Collectively, these data suggest that *Acod1*-deficiency results in more severe pulmonary fibrosis in response to inhaled bleomycin, in comparison to WT controls.

Itaconate controls tissue resident AM metabolism

Recruited, monocyte-derived AMs (Mo-AMs), as opposed to foetally derived tissue resident AMs (Tr-AMs), have been shown to drive the pathogenesis of pulmonary fibrosis in mice (Misharin et al., 2017). However, whether these ontologically discrete cell types are metabolically distinct is not known. In the bleomycin model, recruited Mo-AMs may be identified on the basis of Siglec-F expression: specifically, Tr-AMs were Siglec-F^{hi}, whereas Mo-AMs were Siglec-F^{int} (Misharin et al., 2017). We confirmed these findings by first labelling the lung with a cell permeable die (cell-tracker), prior to the administration of bleomycin (**Supplementary Figure 6A**). Consistent with the published findings, the bulk of Tr-AMs were labelled, whereas the majority of Mo-AMs were unlabeled, indicating recent recruitment (**Supplementary Figure 6B**). In our murine model, proportions of Tr-AMs are diminished at d7 after bleomycin exposure in WT mice, while Mo-AMs make up a high proportion of AMs at d7, reducing by d21 and d42 (**Supplementary Figure 6C**). As we saw the highest number of Mo-AMs at d7 post bleomycin and fibrogenic changes occur in the bleomycin mouse model from day 8 onwards (Moeller et al., 2008), we next assessed the metabolic activity of Mo-AMs and Tr-AMs sorted from bleomycin exposed mice

during this early stage of fibrosis development (d7). In WT mice, Tr-AMs became highly oxidative after bleomycin exposure, whereas Mo-AMs had comparatively diminished baseline oxygen consumption rate (OCR, **Figure 3A** and **B**), showing that Mo-AM and Tr-AM are metabolically distinct (**Supplementary Figure 6D**). Importantly, sorted Mo-AMs highly expressed *Acod1*, in comparison to Tr-AMs from control or bleomycin mice (**Figure 3C**). Since itaconate has recently been shown to control macrophage metabolism and effector functions *in vitro* (Lampropoulou et al., 2016), we next assessed the metabolic impact of CAD deficiency on AM subtypes. Using the Seahorse Mito Stress Test, oxygen consumption rate (OCR) and extracellular acidification rate (ECAR) were measured at baseline and after the sequential addition of 1.5 µM Oligomycin, 2.0 µM FCCP and 0.5 µM Rotenone/Antimycin A. WT Mo-AMs had similar levels of oxidative phosphorylation (OxPhos) and glycolysis (ECAR) compared to *Acod1*$^{-/-}$ cells (**Figure 3D - G**). However, *Acod1*$^{-/-}$ Tr-AMs had reduced OCR (**Figure 3H**), maximal respiration (**Figure 3I**) and spare respiratory capacity (SRC, **Figure 3J**) in comparison to WT Tr-AMs, while basal ECAR remained unchanged (**Figure 3K**). Together these results indicate that during lung fibrosis in mice, recruited Mo-AMs are characterized by a quiescent metabolic phenotype and in contrast, resident Tr-AMs are highly oxidative. Furthermore, CAD expression is a critical regulator of metabolism in tissue resident AMs during lung fibrosis, as itaconate deficiency leads to decreased oxidative phosphorylation. Recently we used single cell sequencing of BAL samples from sex-mismatched lung transplant patients to identify recruited AMs in the human airways (Byrne et al., 2020). Analysis of *ACOD*-expressing cells in a male donor to female recipient, showed a subset of *ACOD1* expressing AMs, which are monocyte derived (MDMs; **supplementary Figure 7A – B**, as they do not express the male cell identifier *RPS4Y1*

but do express the female identifier gene *XIST)*. Consistent with recent work showing itaconate as a regulator of oxidative stress (Mills et al., 2018), pseudo time analysis showed that *ACOD1* increases as MDMs differentiate to mature AMs, while expression of NRF2-target gene *HMOX1* decreases (**Supplementary Figure 7C-D**).

Acod1 deficient tissue resident AMs are more pro-fibrotic post bleomycin

We next assessed how itaconate influenced fibrotic pathways in Mo-AMs and Tr-AMs, sorted from BAL at day 7 post bleomycin challenge. In order to determine whether fibrotic pathways in AMs were impacted by itaconate deficiency, we used a PCR array that interrogates 84 genes involved in the fibrosis cascade (**Supplementary Figure 8A**). Consistent with previous findings (Misharin et al., 2017), Tr-AMs and Mo-AMs differed in their response to bleomycin-induced lung fibrosis, with Mo-AMs comparatively high expressers of genes implicated in fibrotic signaling processes such as *Col1α2*, *Transforming growth factor β 2 (Tgfβ2)* and *Ccr2* (**Supplementary Figure 8A and B**). Comparing Acod1$^{-/-}$ and WT sorted airway macrophages, our data indicate that itaconate deficiency significantly increased gene expression of fibrosis related genes in Tr-AMs (**Figure 4A**), while it downregulated the expression of only two genes in Mo-AMs (**Figure 4B**). In **Figure 4C** and **D** the annotated genes are those that showed significant change in expression or at least 10-fold increase in *Acod1*$^{-/-}$ AMs, compared to WT cells. In Mo-AMs, *IL-1*β*,* and *Integrin linked kinase (Ilk)* were significantly decreased in *Acod1*$^{-/-}$ compared to WT cells, with no significant upregulation in any pro-fibrotic factors (**Figure 4C**). However, in Tr-AMs, pro-fibrotic mediators including *CCAAT enhancer binding protein β (Cebpb), Tgfβr1* and *Smad7* were significantly increased in *Acod1*$^{-/-}$ Tr-AMs compared to WT cells (**Figure 4D**). Examination of cellular morphology (cytospins after Diff-Quik staining) showed that while itaconate-deficient Tr-AMs and Mo-AMs are metabolically and transcriptionally

249 distinct in *Acod1*$^{-/-}$ mice, their size and granularity is unchanged (**Figure 4E**). Together,
250 these data show that itaconate regulates pro-fibrotic pathways in Tr-AMs but not in
251 Mo-AMs.

252 *Adoptive transfer of WT, but not Acod1*$^{-/-}$ *Mo-AMs, into the airways of Acod1*$^{-/-}$
253 *bleomycin treated mice rescued the fibrotic phenotype*

254 As Mo-AMs highly express *Acod1* in comparison to TR-AMs, we next asked whether
255 transfer of WT or Acod1$^{-/-}$ Mo-AMs into an *Acod1*$^{-/-}$ fibrotic environment had differential
256 effects on the course of disease. Sorted Mo-AMs from WT or *Acod1*$^{-/-}$ mice were
257 adoptively transferred into the airways of *Acod1*$^{-/-}$ mice at day 7 post bleomycin
258 (**Figure 5A**). Interestingly, transfer of WT, but not *Acod1*$^{-/-}$ Mo-AMs, into the airways
259 of *Acod1*$^{-/-}$ bleomycin treated mice rescued the fibrotic phenotype, characterized by
260 decreased Ashcroft scores based on Sirius red staining (**Figure 5B and C**) and
261 decreased gene expression of lung *Col3α1* and *Fn1* (**Figure 5D**). However, BAL cell
262 count, total AM and neutrophil numbers as well gene expression of *Col1α1* and *Col4α1*
263 remained unchanged after adoptive transfer (**Figure 5D and Supplementary Figure**
264 **9**). Next, we assessed whether AM phenotype could be altered by adoptive transfer of
265 WT Mo-AMs in to *Acod1*$^{-/-}$ mice. Expression of macrophage activation markers CD11b
266 and MHC II (Byrne et al., 2017; Krausgruber et al., 2011) were assessed in Mo-AMs
267 and Tr-AMs at day 21 post bleomycin with adoptive transfer of WT or *Acod1*$^{-/-}$ Mo-AMs
268 (**Supplementary Figure 9D**). While Tr-AMs showed an increased proportion of
269 activated cells upon adoptive transfer of WT Mo-AMs into *Acod1*$^{-/-}$ (**Figure 5E**) and a
270 decreased proportion of CD11b^{-}/MHCII^{-} cells (**Figure 5F**), this trend was not
271 significantly altered in Mo-AMs (**Figure 5G-H**). Collectively, these results suggest that
272 adoptive transfer of itaconate-sufficient Mo-AMs rescues disease phenotype induced
273 by bleomycin exposure in *Acod1*$^{-/-}$ mice and alters Tr-AM phenotype.

Exogenous itaconate limits human lung fibroblast wound healing

Fibroblasts are the principle effector cell during lung fibrosis and the main source of the excessive extracellular matrix deposition seen during the disease (Kendall and Feghali-Bostwick, 2014), however our data indicate that these cells do not express *Acod1* (*data not shown*). Since macrophages are known to regulate the pro-fibrotic activity of fibroblasts in the lung (Byrne et al., 2016) and itaconate is secreted into the airways (**Figures 1B and 1E**), we next assessed whether itaconate could directly influence fibrosis by limiting the metabolic and pro-fibrotic activity of human lung fibroblasts (HLF). Human lung fibroblasts were cultured in media alone or supplemented with itaconate and assessed after 24h – 72h. After 24h incubation we assessed OCR in response to Oligomycin, FCCP and rotenone/Antimycin A (**Figure 6A**) as well as baseline ECAR (**Figure 6B**) and found that IPF HLFs have increased maximal respiration and spare respiratory capacity compared to healthy HLFs and this effect was ameliorated after stimulation with itaconate (**Figure 6C**). To assess the ability of itaconate to limit fibrosis related functions of HLFs, we carried out proliferation and wound healing assays in the presence or absence of itaconate. After exposure to itaconate, HLFs showed significantly reduced proliferative capacity over 72h in both cells derived from healthy donors (**Figure 6D**) as well IPF patients (**Supplementary Figure 10A**), while the ability to close a standardized wound over a 48h period was decreased in healthy HLFs (**Figure 6E**) but not in IPF fibroblasts (**Supplementary Figure 10B and C**). Furthermore, culture with itaconate downregulated the gene expression of *IL-1*β and *FN-1* in healthy HLFs (**Figure 5F**). Taken together these data suggest that itaconate impacts fibroblast metabolic phenotype, proliferation and wound healing thereby limiting the severity of pulmonary fibrosis.

Inhaled itaconate is anti-fibrotic

Our data show that *ACOD1* expression is reduced in IPF AMs (**Figure 1**), that *Acod1*$^{-/-}$ mice have worsened pulmonary fibrosis in comparison to controls (**Figure 1 and 2**), and that itaconate can limit fibroblast wound healing capacities (**Figure 6**). These data raise the intriguing possibility that exogenous itaconate could improve severity of lung fibrosis. In order to address whether inhaled itaconate is anti-fibrotic, we first determined a dose of itaconate that would not provoke an inflammatory response in murine airways. We found that an inhaled dose of 0.25mg/kg was well tolerated after single (**Supplementary Figure 11A-C**) and/or repeated (*data not shown*) oropharyngeal (OPN) administration in naïve mice and subsequent experiments were carried out at this dose. We administered inhaled (OPN) itaconate or PBS twice a week for two weeks during the fibrotic phase (starting at day 10 post bleomycin) to WT mice (**Figure 7A**); this dosing strategy is in accordance with the American Thoracic guidelines for preclinical assessment of potential therapies for IPF (Jenkins et al., 2017). Subsequently we assessed pathology, fibrosis and lung function at d21 post bleomycin. Remarkably, inhaled itaconate significantly ameliorated all major hallmarks of lung fibrosis, including Ashcroft score based on Sirius red staining (**Figure 7B-C**) expression of *Col4α1* and *Fn1* (**Figure 7C**) and lung airway elastance and compliance (**Figure 7D**). Taken together these results demonstrate that inhaled itaconate significantly improves bleomycin induced pulmonary fibrosis.

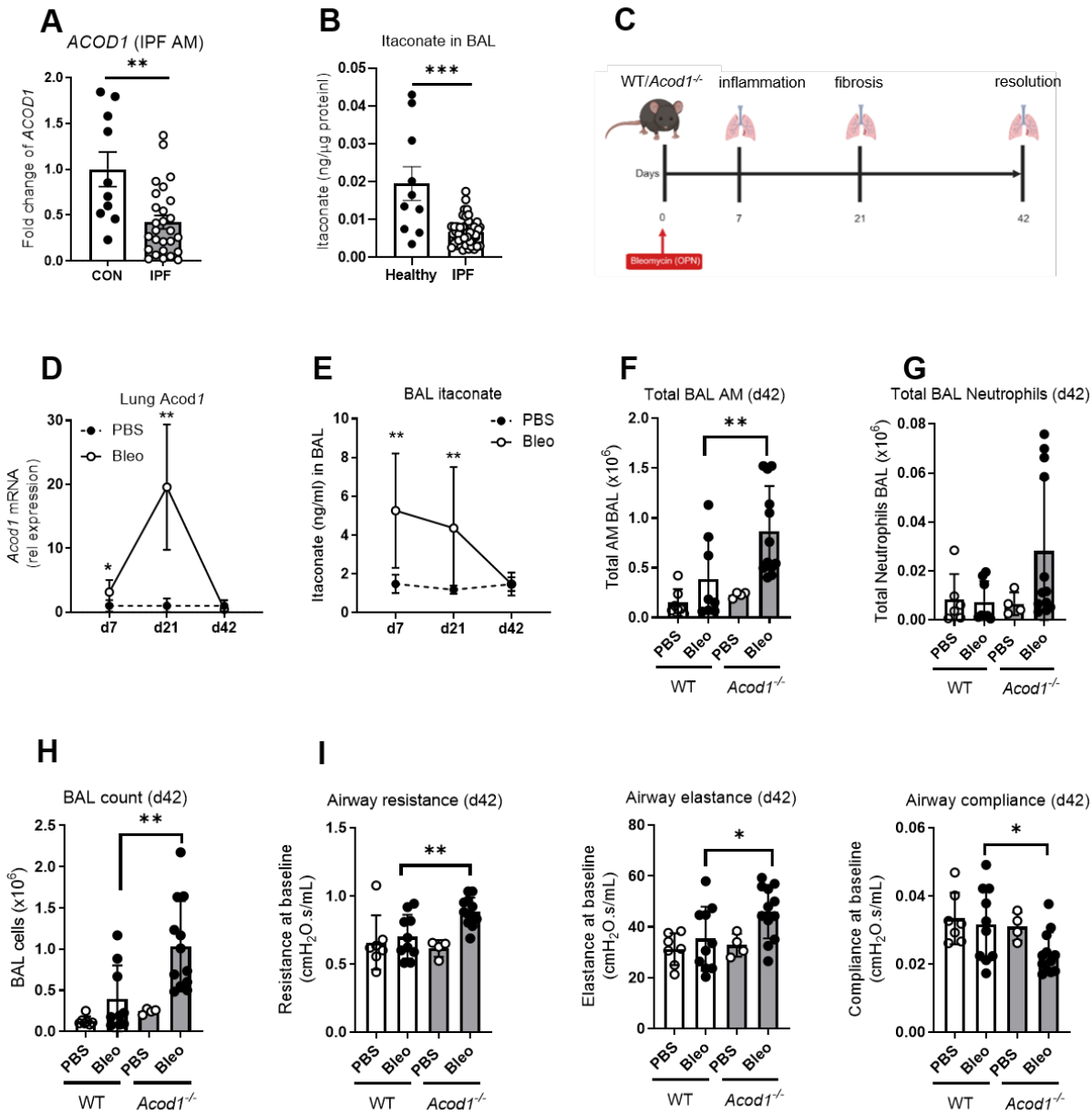

Figure 1: The *ACOD1*/itaconate axis is decreased in IPF and Acod1$^{-/-}$ mice have worsened phenotype upon bleomycin exposure

(A) Gene expression analysis of *ACOD1* in CD206^{+} sorted AMs from human control (n = 10) and IPF (n = 27) donors. *Actb* was used as housekeeping gene. (B) Targeted GC-MS analysis of itaconate in bronchoalveolar lavage (BAL) of human control (n = 10) and IPF (n = 47) donors, normalised to total protein (ng/µg protein). (C) Schematic of dosing regimen. WT or Acod1$^{-/-}$ mice were dosed oropharyngeal with 0.05U

bleomycin or PBS control at day 0 and harvested at day 7, day 21 or day 42 post bleomycin. (D) Gene expression analysis of *Acod1* in lung homogenates of PBS or Bleo dosed mice at day 7, day 21 and day 42 post bleomycin administration; n = 3-8 per group, pooled from two independent experiments. (E) Targeted GC-MS analysis of itaconate in BAL of PBS or Bleo dosed mice at day 7, day 21 and day 42 post bleomycin administration; n = 3-8 per group, pooled from two independent experiments. (F-H) Total BAL cells (F), numbers of BAL AMs (G) and BAL neutrophils (H) in PBS or Bleo dosed WT and *Acod1*$^{-/-}$ mice at day 42; n = 3-8 per group, pooled from two independent experiments. (I) Resistance, elastance and compliance at baseline measured by FlexiVent in PBS or Bleo dosed WT and *Acod1*$^{-/-}$ mice at day 42 (PBS n = 4 – 7, Bleo n = 10 -12), pooled from two independent experiments and representative of n=3 individual experiments. Data presented as mean ± S.D. Statistical significance tested by Mann-Whitney U test or One-Way ANOVA + Sidak's multiple comparison test , *$P < 0.05$, ** $P < 0.01$, *** $P < 0.005$, **** $P < 0.001$.

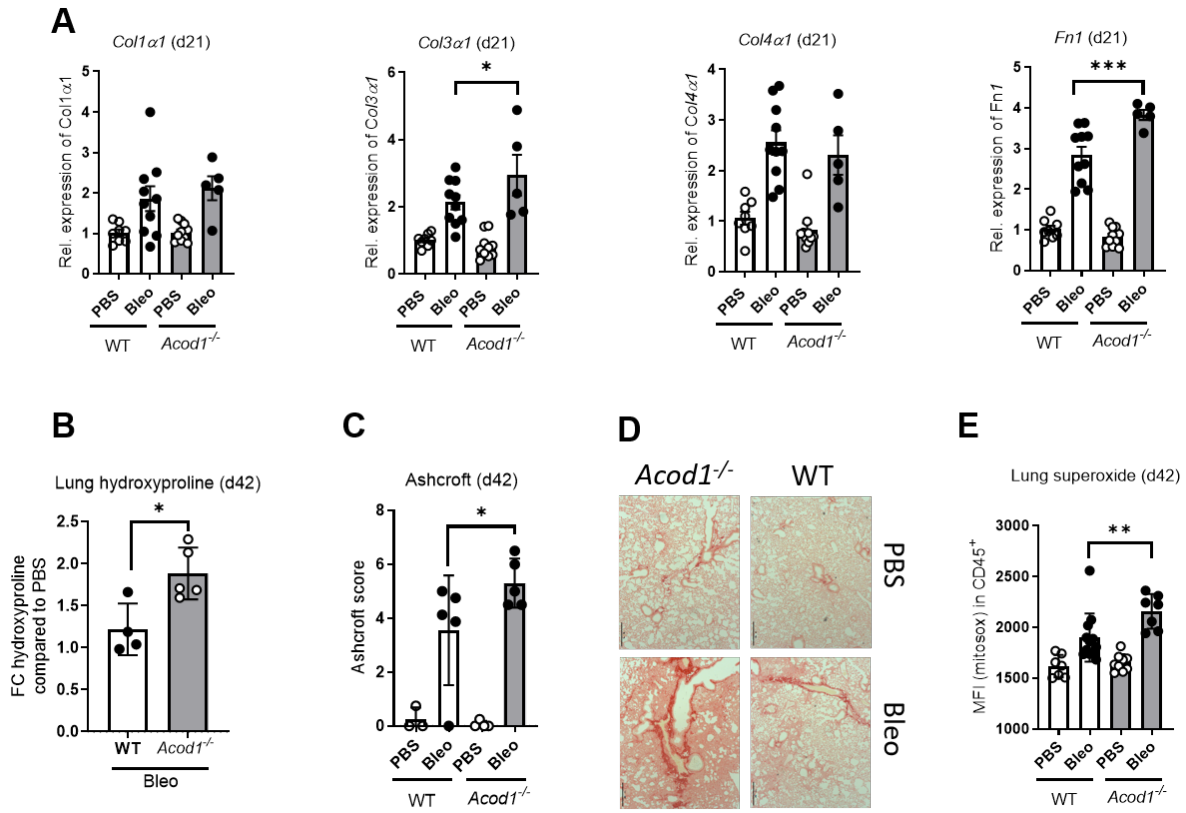

Figure 2: *Acod1*$^{-/-}$ mice have worsened fibrotic phenotype at late time point

(A) Gene expression analysis of *Col1α1 Col3α1, Col4α1* and *Fn1* in lung homogenate of PBS or Bleo dosed WT and *Acod1*$^{-/-}$ mice at day 21 (n = 3-8 per group). *Actb* was used as housekeeping gene. Pooled from two independent experiments. (B) Fold change hydroxyproline increase in bleomycin compared to PBS in WT and *Acod1*$^{-/-}$ mice at day 42 post bleomycin (n = 4-5 per group), representative of three experiments. (C-D) Ashcroft score (C) and representative images (D) of lung slices of PBS or Bleo dosed mice at day 42 post bleomycin stained with Sirius Red, scored blinded by 3-5 individuals. (E) MFI of MitoSOX red superoxide stain in lungs of PBS or Bleo WT and *Acod1*$^{-/-}$ mice at day 42 post Bleo (n = 7-12 per group), pooled from two independent experiments and representative of n = 3 individual experiments.

Data presented as mean ± S.D. Statistical significance tested by Mann-Whitney U test or One-Way ANOVA + Sidak's multiple comparison test , *$P < 0.05$, ** $P < 0.01$.

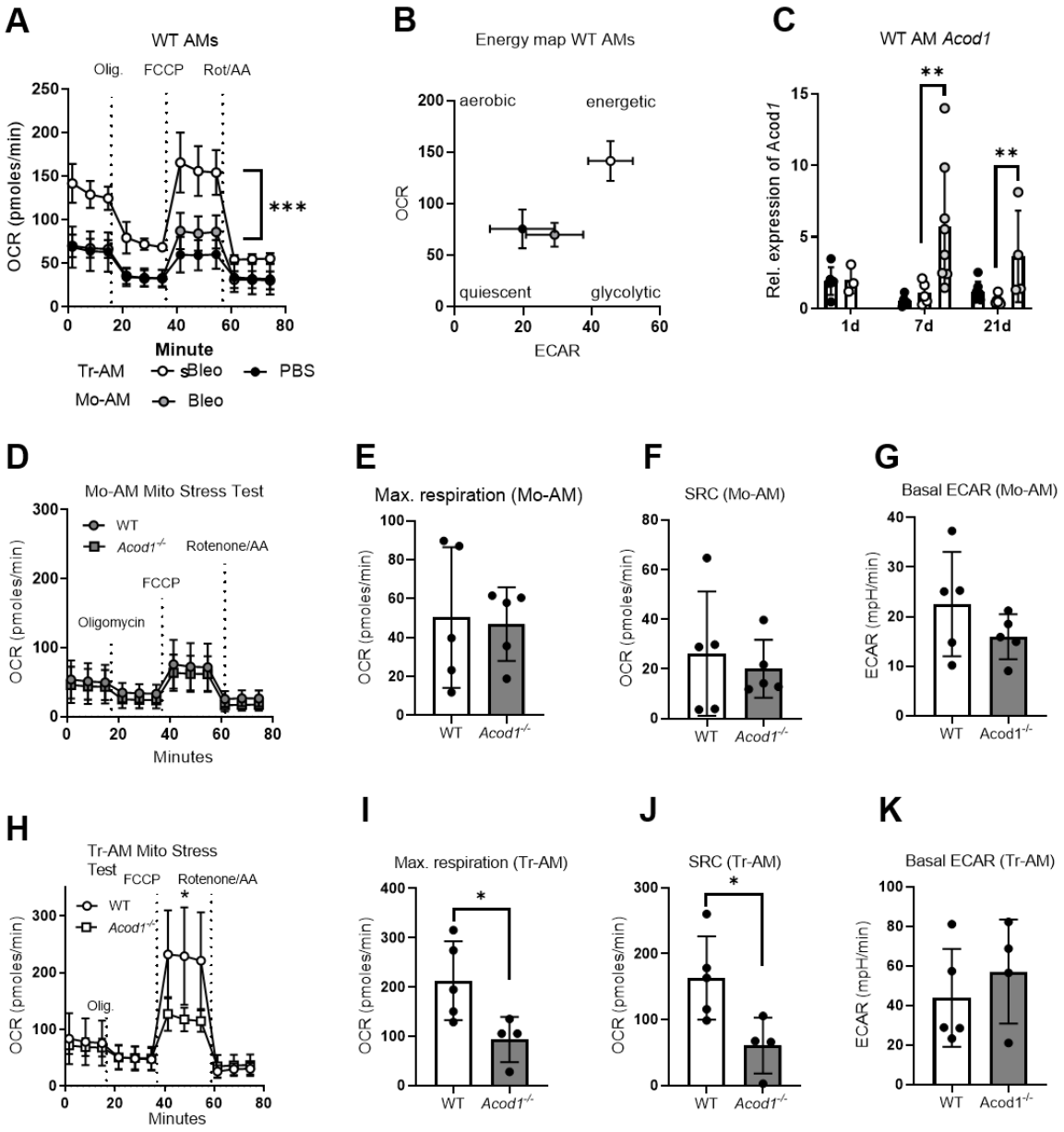

Figure 3: Itaconate controls tissue resident AM metabolism

(A) Analysis of the oxygen consumption rate (OCR) of PBS tissue resident-AM (Tr-AM) (n = 3), Bleo Tr-AM (n = 4) and Bleo monocyte recruited-AM (Mo-AM, n = 5) during mitochondrial stress test, assessed after injection of Oligomycin, FCCP and

Rotenone/Antimycin A; representative of three independent experiments. (B) Energy map of indicating overall energy state of PBS Tr-AM, Bleo Tr-AM and Bleo Mo-AM; four energy states are shown: quiescent, energetic, aerobic and glycolytic. Same n numbers as in A. (C) Gene expression analysis of *Acod1* in BAL PBS Tr-AM, Bleo Tr-AM and Bleo Mo-AM at day 1, day 7 and day 21 (n = 4-7 per group) post bleomycin. *Actb* was used as housekeeping control. Pooled from three independent experiments. (D) Analysis of the OCR of Bleo WT Mo-AM (n=5) and *Acod1*$^{-/-}$ Mo-AM (n=5) during mitochondrial stress test, assessed as in A; data from two experiments pooled. (E) Maximal respiration during mitochondrial stress test (D), defined as the maximal oxygen consumption rate after addition of FCCP. (F) Spare respiratory capacity (SRC) during mitochondrial stress test (D), defined as subtraction of basal from maximal OCR. (G) Basal extracellular acidification rate (ECAR) as surrogate for glycolysis during mitochondrial stress test (D). (H) Analysis of the OCR of Bleo WT Tr-AM (n = 4) and *Acod1*$^{-/-}$ Tr-AM (n = 4) during mitochondrial stress test, assessed as in A; data from two experiments pooled. (I) Maximal respiration during mitochondrial stress test (G), calculated as in (E). (J) SRC during mitochondrial stress test (G), defined as in (F). (K) Basal extracellular acidification rate (ECAR) as surrogate for glycolysis during mitochondrial stress test (H).

Tr-AM and Mo-AM were sorted at day 7 post bleomycin. Data presented as mean ± S.D. Significance tested by One-Way ANOVA + Sidak's multiple comparison test, *P < 0.05, ** P < 0.01, *** P < 0.001. Each data point represents 2 - 3 mice pooled.

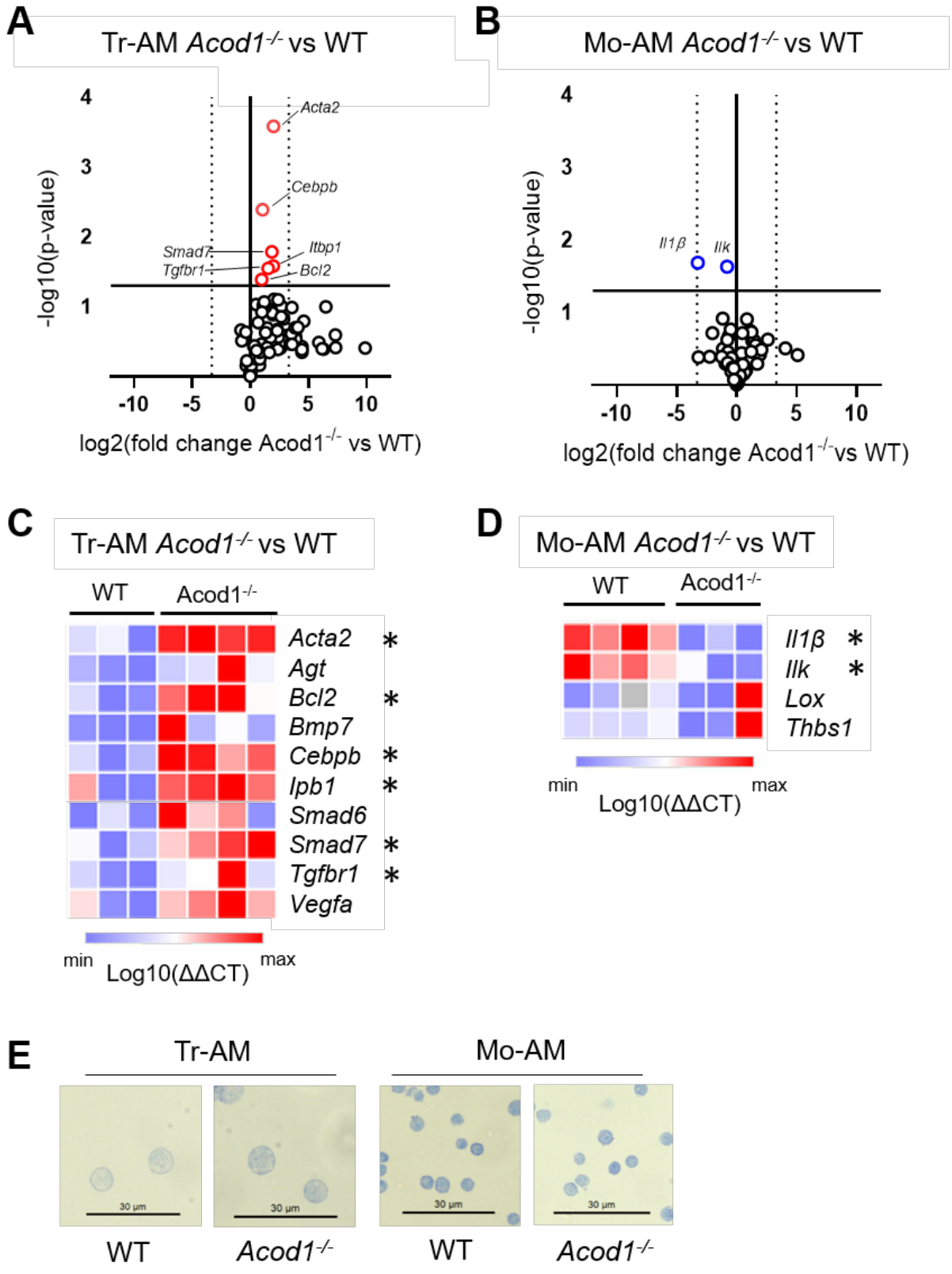
A
Tr-AM Acod1-/- vs WT
-log10(p-value)
log2(fold change Acod1-/- vs WT)
Acta2
Cebpb
Itbp1
Bcl2
Smad7
Tgfbr1
B
Mo-AM Acod1-/- vs WT
-log10(p-value)
log2(fold change Acod1-/-vs WT)
Il1β
Ilk
C
Tr-AM Acod1-/- vs WT
WT
Acod1-/-
Acta2 *
Agt
Bcl2 *
Bmp7
Cebpb *
Ipb1 *
Smad6
Smad7 *
Tgfbr1 *
Vegfa
min
Log10(ΔΔCT)
max
D
Mo-AM Acod1-/- vs WT
WT
Acod1-/-
Il1β *
Ilk *
Lox
Thbs1
min
Log10(ΔΔCT)
max
E
Tr-AM
Mo-AM
30 µm
WT
Acod1-/-
WT
Acod1-/-

385

386

Figure 4: *Acod1*-deficient tissue resident AMs are more pro-fibrotic post bleomycin

(A – B) Volcano plots showing differentially expressed genes in WT vs *Acod1*$^{-/-}$ Tr-AM (A) and Mo-AM (B), 7 days post bleomycin exposure (n = 3 – 4 per group). Genes significantly ($p < 0.05$) up-regulated in WT vs *Acod1*$^{-/-}$ highlighted in red, while genes significantly downregulated are shown in blue. (C–D) Heat map representation of murine fibrosis gene array of FACS sorted Mo-AM (C) and Tr-AM (D) from WT and *Acod1*$^{-/-}$ mice. Data shown as log10 of ΔΔCT WT vs *Acod1*$^{-/-}$. (E) Representative images of FACS sorted Tr-AM and Mo-AM WT and *Acod1*$^{-/-}$ mice after cytospin and Diff-Quick staining. Significance tested by Two-tailed T-test *$P < 0.05$.

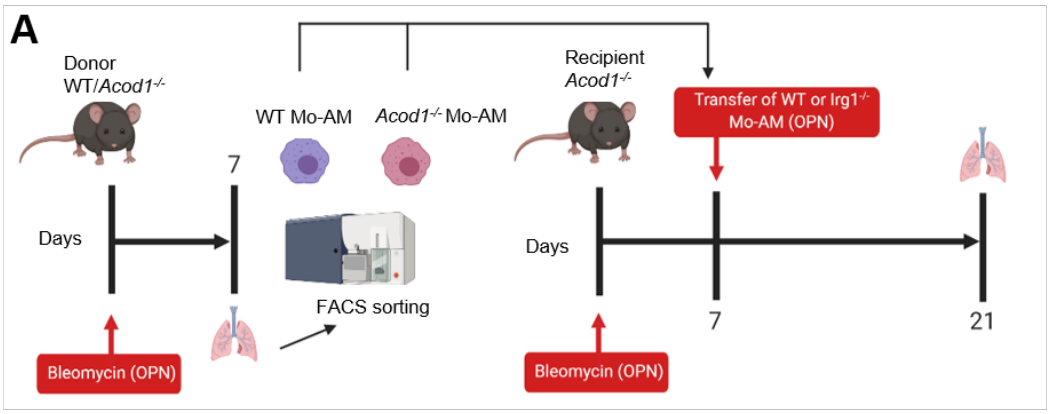
A
Donor
WT/Acod1-/-
WT Mo-AM
Acod1-/- Mo-AM
Recipient
Acod1-/-
Transfer of WT or Irg1-/-
Mo-AM (OPN)
Days
7
FACS sorting
Days
7
21
Bleomycin (OPN)
Bleomycin (OPN)

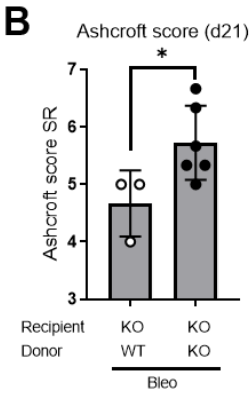
B
Ashcroft score (d21)
Ashcroft score SR
Recipient KO KO
Donor WT KO
Bleo

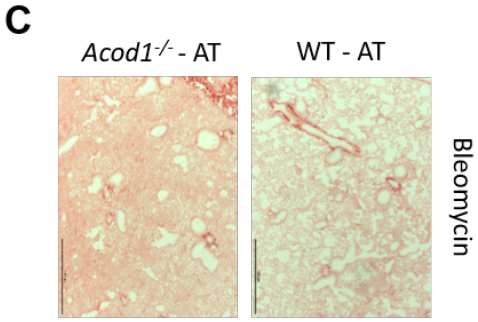
C
Acod1-/- - AT
WT - AT
Bleomycin

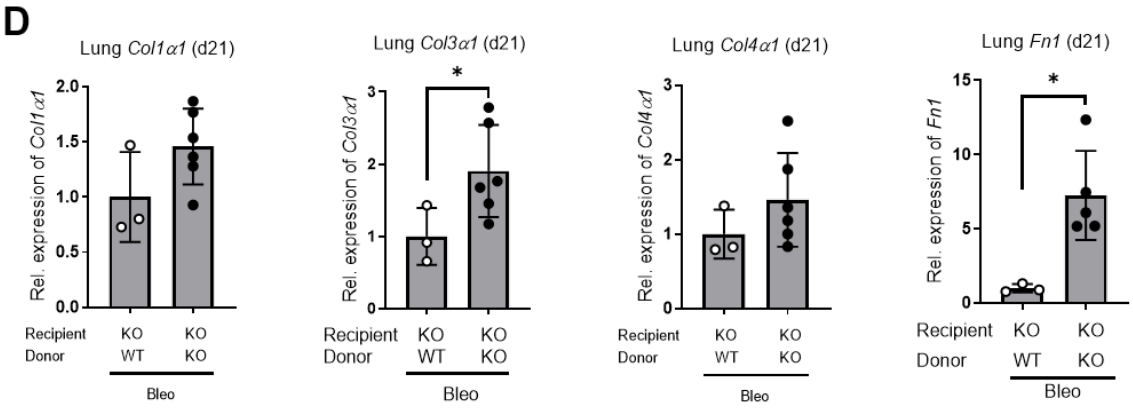
D
Lung Col1α1 (d21)
Rel. expression of Col1α1
Lung Col3α1 (d21)
Rel. expression of Col3α1
Lung Col4α1 (d21)
Rel. expression of Col4α1
Lung Fn1 (d21)
Rel. expression of Fn1
Recipient KO KO
Donor WT KO
Bleo

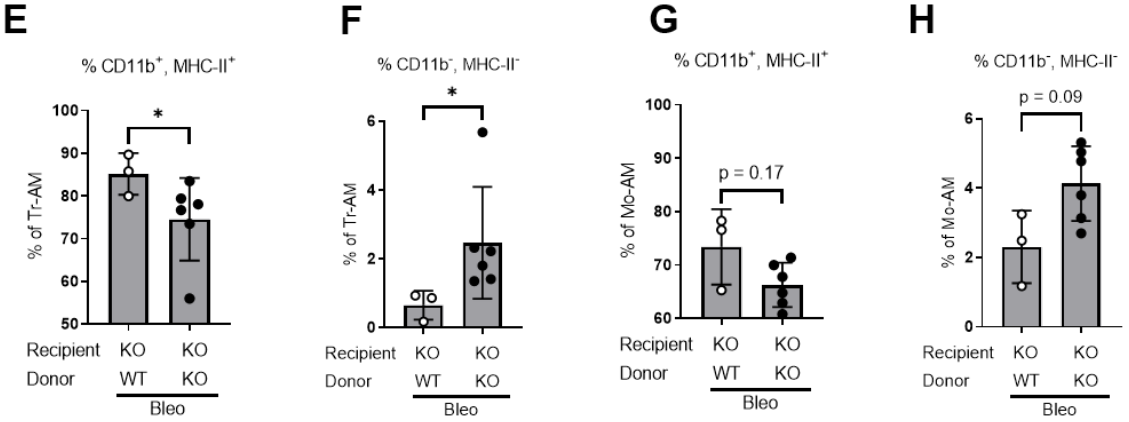
E
% CD11b+, MHC-II+
% of Tr-AM
F
% CD11b-, MHC-II-
% of Tr-AM
G
% CD11b+, MHC-II+
p = 0.17
% of Mo-AM
H
% CD11b-, MHC-II-
p = 0.09
% of Mo-AM
Recipient KO KO
Donor WT KO
Bleo

Figure 5*:* Adoptive transfer of WT Mo-AMs improves pulmonary fibrosis and rescues tissue resident AM phenotype in Acod1$^{-/-}$ mice post bleomycin

(A) Schematic of dosing regimen and adoptive transfer. WT or *Acod1*$^{-/-}$ mice were dosed oropharyngeal with 0.05U bleomycin at day 0, Mo-AMs were FACS sorted at day 7 post bleomycin and transferred into *Acod1*$^{-/-}$ mice via the oropharyngeal route. Mice were then harvested after further 14 days, at day 21 post initial bleomycin exposure. (B–C) Ashcroft score (D) and representative images (E) of lung slices of *Acod1*$^{-/-}$ mice adoptively transferred with WT or *Acod1*$^{-/-}$ Mo-AMs; day 21 post bleomycin stained with Sirius Red, scored blinded by 3-5 individuals. (D) Gene expression analysis of *Co1a1, Col3a1, Col4a1* and *Fn1* in lung homogenate of *Acod1*$^{-/-}$ mice adoptively transferred with WT or *Acod1*$^{-/-}$ Mo-AMs (n = 3 – 6 per group); day 21 post bleomycin, *Actb* was used as housekeeping gene. (E-H) Fraction of CD11b^{+}/MHC II^{+} and CD11b^{-}/MHC II^{-} Tr-AM (E-F) and Mo-AM (G-H) in BAL of *Acod1*$^{-/-}$ mice adoptively transferred with WT or *Acod1*$^{-/-}$ Mo-AMs; day 21 post bleomycin. Data presented as mean ± S.D. Significance tested by Mann Whitney U test, **P* < 0.05.

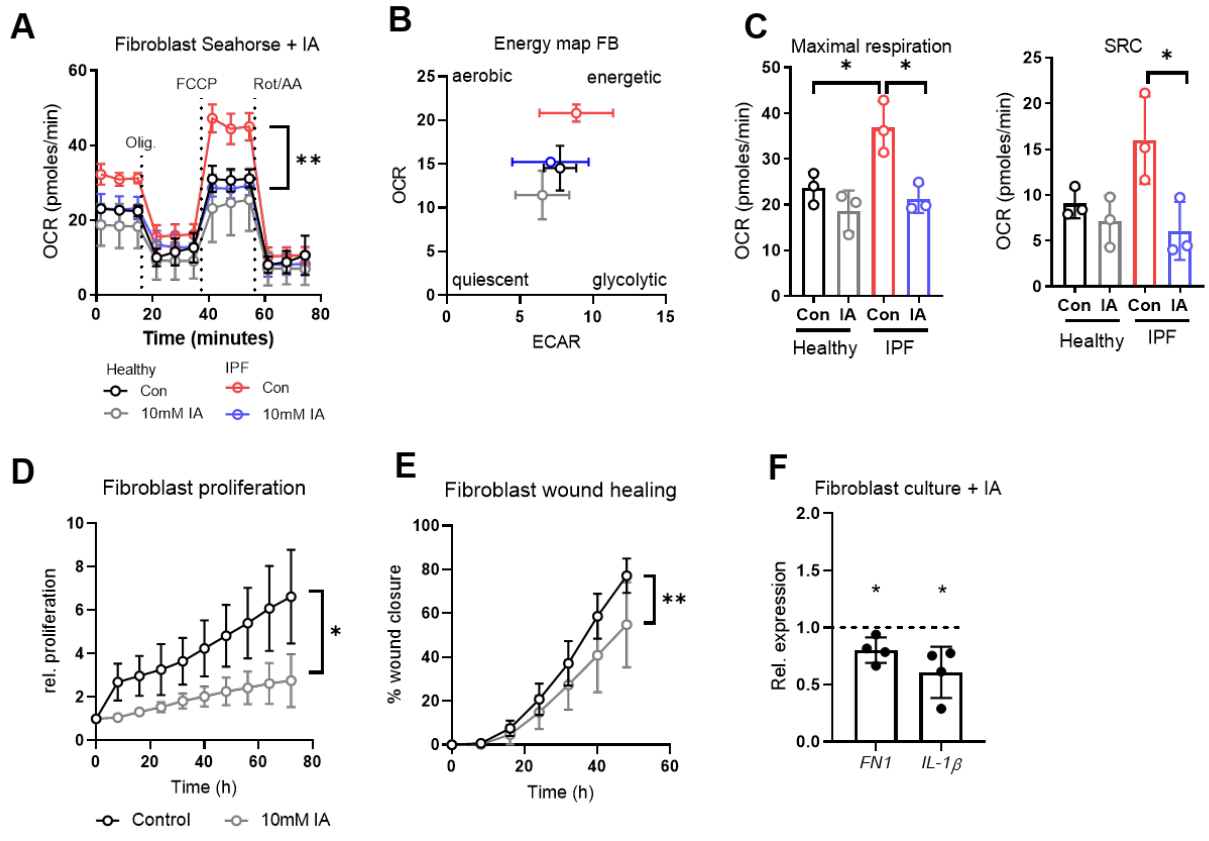

415

416 **Figure 6: Exogenous itaconate limits human lung fibroblast wound healing**

417 (A) Analysis of the OCR of healthy or IPF primary human lung fibroblasts stimulated
418 for 24h with either RPMI medium (con) or 10mM itaconate (IA) during mitochondrial
419 stress test, assessed after injection of Oligomycin, FCCP and Rotenone/Antimycin A
420 (all groups n = 3). (B) Energy map of (A) showing four energy states during
421 mitochondrial stress test: quiescent, energetic, aerobic and glycolytic. Same n
422 numbers as in A. (C) Maximal respiration and spare respiratory capacity (SRC) during
423 mitochondrial stress test (A). Maximal respiration defined as the maximal oxygen
424 consumption rate after addition of FCCP; SRC defined as subtraction of basal from
425 maximal OCR. (D) Proliferation rate of healthy (n = 3) human primary lung fibroblasts
426 stimulated with 10mM itaconate or vehicle control measured using the JULI Stage
427 system. (E) Wound healing capacity of healthy (n = 3) human primary lung fibroblasts
428 stimulated with 10mM itaconate or vehicle control measured using the JuLI Stage

system. Two-tailed, unpaired t-test of area under the curve. (F) Gene expression analysis of FN1 and IL-1β in healthy human primary lung fibroblasts stimulated for 24h with 10mM itaconate or vehicle control. IA = itaconate. Data presented as mean ± S.D. Significance was tested by One Way ANOVA + Sidak's multiple comparison test (A – C), Mann Whitney U test of arear under the curve (D – E) or one-sample t-test against value of 1.0 (F). *P < 0.05, ** P < 0.01.

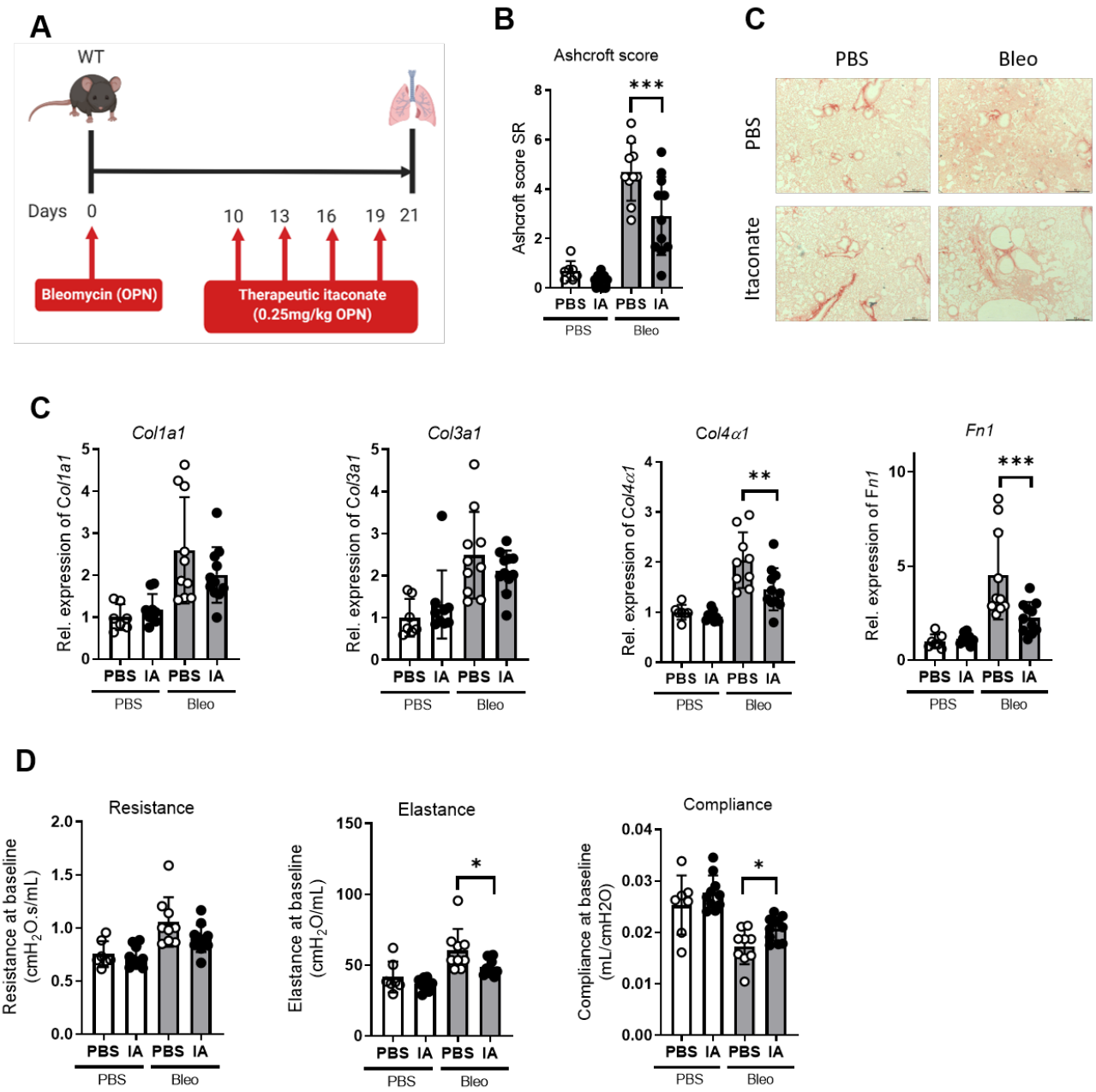

436

437 **Figure 7: Inhaled itaconate is anti-fibrotic**

438 (A) Schematic of dosing regime using 8-10 week old C57Bl/6 mice. 0.05U Bleomycin
439 or PBS control and 0.25mg/kg itaconate or PBS control was administered
440 oropharyngeal at indicated time points and mice were harvested at day 21 post
441 bleomycin. (B - C) Ashcroft score and representative images (C) of lung slices stained
442 with Sirius Red, scored blinded by 3-5 individuals. (D) Gene expression analysis of
443 *Col1α1, Col3α1, Col4α1* and *Fn1* in lung homogenate; *Actb* was used as

housekeeping control. Pooled from two independent experiments. (E) Resistance, elastance and compliance at baseline measured by FlexiVent in PBS and bleomycin dosed mice treated with 0.25mg/kg itaconate or vehicle control. Pooled from two independent experiments.

Data presented as mean ± S.D.; n = 7 – 11 per group. Significance was tested by by One-Way ANOVA + Sidak's multiple comparison test * $P < 0.05$.

Discussion

In this study, we identify a critical role for the *Acod1*/itaconate pathway in the pathogenesis of pulmonary fibrosis. We show that the *ACOD1*/itaconate pathway is significantly disrupted in IPF and that *Acod1*$^{-/-}$ mice have more severe lung disease in a murine model of pulmonary fibrosis. *Acod1* influences fibrotic responses in AMs as *Acod1*$^{-/-}$ AMs demonstrated impaired metabolism and enhanced expression of pro-fibrotic genes, while adoptive transfer of WT monocyte-recruited AMs into the lungs of *Acod1*$^{-/-}$ improved bleomycin induced pulmonary fibrosis and altered Tr-AM phenotype. *Ex vivo* culture of human fibroblasts with itaconate reversed their metabolic reprogramming in IPF and decreased both proliferation and wound healing capacity. We also show that therapeutic administration of inhaled itaconate *in vivo* ameliorates bleomycin-induced pulmonary fibrosis in mice. Thus, our work suggests the *ACOD1*/itaconate axis as a novel, endogenous anti-fibrotic pathway which is dysregulated during IPF. Our data highlight the prospect of novel therapeutic strategies, which directly promote *ACOD1*/itaconate and pharmacological approaches which deliver itaconate or its derivatives as anti-fibrotic agents.

It is now well established that in mice, lung-resident AMs maintain their populations *via* proliferation *in situ* during homeostasis and that a second population of ontologically distinct Mo-AMs are recruited from peripheral monocytes during ongoing inflammatory responses. Misharin and colleagues recently showed that monocyte-derived, recruited AMs rather than foetally derived tissue-resident AMs were essential for the development of pulmonary fibrosis in murine models, whereas deletion of tissue-resident AMs had no effect on the disease (Misharin et al., 2017). Our data indicate that *Acod1* is differentially expressed in Tr-AMs and Mo-AMs and that these cell types are metabolically distinct. Furthermore, as itaconate synthesis *via Acod1* is

an anti-fibrotic pathway expressed in Mo-AMs, and these have previously been suggested as drivers of pulmonary fibrosis (Misharin et al., 2017), our data indicates that there is some functional diversity within Mo-AM populations, which may be determined in part, by *Acod1* expression. Of note, our recent findings, which lineage traced AM populations in the human lung using BAL from sex-mismatched lung transplant patients, have shown that the majority of AMs in the adult lung are monocyte derived rather than tissue resident cells (Byrne et al., 2020). Therefore, our finding that *Acod1* is highly expressed in Mo-AM populations in mice is particularly relevant.

AMs play an important role in defending the lung environment from inhaled threats and are key sentinels of pulmonary homeostasis. AM phenotype is a critical component of lung immunity and manipulation of AM phenotype can have drastic consequences for lung health (Byrne et al., 2017). Itaconate has emerged as a key autocrine immunoregulatory component involved in activation of bone-marrow derived macrophages (BMDMs), however there is little known regarding the specific role of itaconate in highly specialized tissue resident macrophage populations, such as those found in the airways, during chronic disease. Several reports have described itaconate as a protective pathway against infection in the lung. Ren *et al.* found that RSV infection induced *ACOD1* expression in A549 cells (an immortalized human alveolar epithelial cell line derived from an adenocarcinoma) and in the lung tissues of RSV-infected mice; furthermore *Acod1* knockdown blocked RSV-induced ROS production, pro-inflammatory cytokine gene expression and immune cell infiltration (Ren et al., 2016). Using global metabolomics profiling Shin *et al.* showed that rodents infected with *Mycobacterium tuberculosis* (MTb) had elevated itaconate levels in lung, but not spleen extracts (Shin et al., 2011). Itaconate is a critical component of pulmonary responses to MTb infection as both global *Acod1*$^{-/-}$ and myeloid-specific *Acod1*$^{-/-}$

knockouts rapidly succumb to infection (Nair et al., 2018). Collectively, these data outline a potential role for the *ACOD1*/itaconate axis in the lung during infection. Our data in the context of pulmonary fibrosis highlight itaconate as a critical component of respiratory immunity.

While we show that in the bleomycin mouse model, itaconate is increased in the BAL during the inflammatory stage and recovers to baseline levels during the late phase, in human AMs *ACOD1* is highly expressed at homeostasis and disrupted during pulmonary fibrosis. This is particularly pertinent as there are a dearth of data regarding the role of itaconate during human disease and as a predisposition towards development of chronic lung disease. Consistent with our findings Meiser *et al* recently reported that itaconate was not detectable in plasma or urine of septic patients or in BAL of patients with pulmonary inflammation, including patients with COPD and sarcodoisis (Meiser et al., 2018). We show for the first time that itaconate can directly influence human lung fibroblast phenotype and function *in vitro*, which might be part of the mechanism behind the improved lung function, collagen gene expression and deposition we observed upon administration of inhaled itaconate during the fibrotic phase of the bleomycin mouse model. Our findings indicate that itaconate could mediate paracrine effects on other stromal or immune cells types as it is actively secreted at homeostasis and thus may have implications for chronic diseases of the lung or other tissues, in which fibrosis plays a role.

Our data show that *ACOD1* is expressed in AMs of healthy controls and expression is decreased in AMs from IPF patients. Of note, *ACOD1* is not well represented in the IPF Cell Atlas single cell RNAseq datasets (Habermann et al., 2019; McDonough et al., 2019; Morse et al., 2019; Reyfman et al., 2019), this might be due to several factors regarding sample processing protocols, sequencing depth of single cell approaches

and the severity of fibrosis patients investigated. IPF Cell Atlas datasets were generated from enzymatic digestion whole lung homogenates rather than from lavage, which is likely a major confounder for the study of metabolic processes. Furthermore, IPF Cell Atlas patients were end-stage IPF (or other ILD) patients, while in contrast, our study evaluated expression of *ACOD1* in patients undergoing diagnostic bronchoscopy. Finally, the control lungs reported in the IPF Cell Atlas studies were either declined for organ donation or transplant donors, whereas control samples from our study were obtained from BAL of healthy volunteers. For our murine studies, we have reported lung function, collagen/fibronectin gene expression, Ashcroft scoring on Sirius red (collagen stain) stained histology slices, in order to assess the role of *Acod1*/itaconate in pulmonary fibrosis. We have not reported pulmonary hydroxyproline levels for adoptive transfer and therapeutic studies, due to limited access to our laboratories as a result of the Covid-19 pandemic.

In conclusion, this work defines a novel regulatory pathway, which is impaired during fibrotic lung disease. The novel relationships between *ACOD*1, airway macrophages and fibrosis reported here have the potential to impact therapies for IPF and highlight *ACOD1*, itaconate or its metabolites as molecular targets for the treatment of fibrotic lung diseases.

Materials and methods

Lead Contact and Materials Availability

Requests for further information and reagents may be directed and will be fulfilled by the corresponding author, Dr. Adam J. Byrne (a.byrne@imperial.ac.uk).

Experimental Model and Subject Details

Human bronchoalveolar lavage

Bronchoscopy of the right middle lobe was performed after informed consent as approved by an external Research Ethics Committee for ILD subjects (Ref. Nos. 10/H0720/12 and 15/SC0101) and healthy control subjects (Ref. No. 15-LO-1399) according to the Royal Brompton Hospital protocol (Royal Brompton & Harefield NHS Foundation Trust, 2016). Bronchoscopies were performed with subjects under a light sedation with midazolam in combination with local anesthesia with lidocaine. Four 60-ml aliquots of warmed sterile saline were instilled in the right middle lung lobe and aspirated by syringe and lavage aliquots collected after each instillation were pooled for each patient. Volume and BAL appearance were recorded for all samples.

Cell culture

Primary human lung fibroblasts were isolated from lung resections of patients undergoing lung cancer surgery or lung transplantation performed after informed consent as approved by an external Research Ethics Committee (REC 15/SC0101) according to the Royal Brompton Hospital protocol (Royal Brompton & Harefield NHS Foundation Trust, 2016) and cultured in complete Dulbecco's modified eagle medium (10% FBS, 100U/ml penicillin/streptomycin) (Gibco, ThermoFisher) to passage four. Human bronchial epithelial cells (HBE) were obtained from bronchial brushings during the bronchoscopy after informed consent and approved by an external Research Ethics Committee for ILD subjects (Ref. Nos. 10/H0720/12 and 15/SC0101). HBEs were cultured in xxx medium to passage four. MACS enriched human AM were cultured in complete RPMI (10% FBS, 100U/ml penicillin/streptomycin, Gibco, ThermoFisher) for 24 hrs. Fibroblasts and AM were cultured with 10mM itaconate in

complete medium for 24hrs prior to cell lysis in RLT buffer (QIAGEN) containing 1% 2-Mercaptoethanol (Sigma Aldrich).

Mice

Acod1$^{-/-}$ (C57BL/6NJ-Acod1^(em1J)/J, JAX stock number 029340) mice and littermate controls were bred on a C57BL/6 background. Unless otherwise stated, all mice were between 8 and 12 weeks of age. Mice were housed in specific-pathogen-free conditions and given food and water *ad libitum*. All procedures were approved by the United Kingdom Home Office and conducted in strict accordance with the Animals (Scientific Procedures) Act 1986. The Imperial College London Animal Welfare and Ethical Review Body (AWERB) approved this protocol. All surgery was performed under ketamine and sodium pentobarbital anaesthesia and all efforts were made to minimize suffering. Mice were administered either 0.05U (1U/ml solution dissolved in PBS) of bleomycin sulphate (Sigma Aldrich) or 50µl PBS via the oropharyngeal route at day 0 and culled after 7, 21 or 42 days. For therapeutic experiments mice were administered 0.25mg/kg (1mM solution dissolved in PBS, 50µl) itaconic acid (Sigma Aldrich) or PBS via the oropharyngeal route twice a week, beginning 10 days after of bleomycin administration.

Method Details

Subject demographics

76 IPF patients and 17 control subjects were recruited. Demographic and clinicopathological features are detailed in **Supplementary Tables 1 and 2**. Healthy volunteers had no self-reported history of lung disease, an absence of infection within the last 6 months and normal spirometry.

Human AM isolation

$1x10^7$ BAL cells were stained with anti-CD206 (Biolegend) and Human TruStain FcX block (Biolegend) for 15 minutes at 4°C in 0.5% FBS/2mM EDTA in PBS prior to incubation with MACS anti-Cy7 microbeads (Miltenyi Biotec) for 15 minutes at 4°C. Cells were enriched in MACS magnetic separation column (Miltenyi Biotec) and purity was confirmed on a representative subset (n = 29) by flow cytometry.

Single cell RNA sequencing

Viable cryopreserved BAL cells were sorted on a BD Influx sorter (Becton Dickinson) as previously described (Byrne et al., 2020) and retained on ice. Briefly, cells at a concentration of 800 – 1,000 cells/µl were loaded onto 10x Genomics single cell 3' chips along with the RT mastermix (Chromium Single Cell 3' Library, v2, PN-120233, 10X Genomics) according to manufacturer's instructions to generate single-cell gel beads in emulsion. RT was performed using a C1000 Touch Thermal Cycler with a Deep Well Reaction Module (Bio-Rad; 55°C for 2 h; 85°C for 5 min; hold 4°C). DynaBeads (MyOne Silane Beads, Thermo Fisher Scientific) and SPRIselect beads (Beckman Coulter) were used to purify and recover cDNA., which was subsequently amplified (98°C for 3 min; 12 times - 98°C for 15 s, 67°C for 20 s, 72°C for 60 s); 72°C for 60 s; hold 4°C). Amplified cDNA was sheared to ~200 bp with a Covaris S2 instrument using the manufacturer's recommended parameters. Sequencing libraries were generated with unique sample indices and sequenced on a Illumina NewtSeq 500 (NextSeq control software v2.0.2/ Real Time Analysis v2.4.11) using a 150-cycle NextSeq 500/550 High Output Reagent Kit v2 (FC-404-2002; Illumina) in stand-alone mode as follows: 98 bp (read 1), 14 bp (I7 index), 8 bp (I5 index), and 485 10 bp (read 2).

The Cell Ranger Single Cell Software Suite (10X Genomics, v2.0.0) was used to process the sequencing data into transcript count tables. Raw base call files were demultiplexed using the Cell Ranger mkfastq programme into sample-specific FASTQ files, which were then processed using the Cell Ranger count pipeline. Subsequent analysis was performed as described previously (Byrne et al., 2020).

Determination of itaconate by Gas Chromatography/Mass Spectrometry

Freeze dried BAL samples were spiked with d_3-labelled methylmalonic acid (d3-MMA, synthesized in house) and derivatized with 30µl methoxyamine hydrochloride (Sigma-Aldrich, 20mg/ml in pyridine, 40°C for 20min) to modify any carbonyls (multi-component method). After cooling, 70µl of N,O-bis(trimethylsilyl)trifluoroacetamide containing 1% trimethylchlorosilane (BSTFA Sigma-Aldrich) were added and the mixture incubated for 30 minutes at 60°C to effect trimethylsilylation of the hydroxy functions. Finally, the supernatants from centrifuged reaction mixtures were transferred to injection vials. GC/MS analysis was performed on an Agilent 6890 gas chromatograph coupled to a 5973 MSD quadrupole mass spectrometer. Samples were injected in splitless mode with the inlet maintained at 280°C. Separation of the derivatives was performed on a DB-1701 capillary column 30m x 250µm x 0.25µm (Agilent Technologies) using a three-stage temperature program to optimize the separation. Mass spectral data was acquired by selected ion monitoring (SIM) of m/z 259 (quantifier) and m/z 215 (qualifier) at approx. 6 min retention time. A five-level calibration plot was constructed over the concentration range 0-16 ng/ml. Quantitation was achieved by interpolation using the regression equation of the calibration curve. All data processing and concentration calculations were performed using Agilent MassHunter (v. B.07.01) software.

Murine Lung Function Assessment

Lung function measurements were performed using the Flexivent system (Scireq, Montreal, Canada). After induction of anaesthesia with an i.p. injection of Pentobarbitone (50 mg/Kg, Sigma, UK) and i.m. injection of Ketamine (200 mg/Kg) (Fortdodge Animal Health Ltd, Southampton, UK), mice were tracheotomised and attached to the Flexivent ventilator via a blunt-ended 19-gauge needle. Mice were ventilated using the following settings; tidal volume of 7 ml/Kg body weight, 150 breaths/minute; positive end-expiratory pressure approximately 2cm H_2O. Standardisation of lung volume history was done by performing two deep inflations. Subsequently, measurements of dynamic resistance, dynamic elastance and dynamic compliance were determined using the snapshot-150 perturbation, a single frequency sinusoidal waveform. Resultant data was fitted using multiple linear regression to the single compartment model to determine the above parameters.

Murine BAL and Lung Cell Recovery

In order to obtain BAL, the airways of the mice were lavaged three times with 0.4 ml of PBS via a tracheal cannula. BAL fluid was centrifuged (700 X g, 5 min, 4°C); cells were resuspended in 0.5 ml complete media (RPMI + 10% fetal calf serum [FCS], 2 mM L-glutamine, 100 U/ml penicillin/ streptomycin). Cells were counted and pelleted onto glass slides by cytocentrifugation (5×10^4 cells/slide). To disaggregate cells from lung tissue, one finely chopped left lobe of lung was incubated at 37°C for 1 h in digest reagent (0.15 mg/ml collagenase type D, 25 µg/ml DNase type I) in complete RPMI media. The recovered cells were filtered through a 70-µm nylon sieve, washed twice, resuspended in 1ml complete media, and counted in a haemocytometer prior to cytocentrifugation; lung cell counts are quoted as total cell number/ml of this suspension.

Flow cytometry

Cells were stained with near IR fixable live/dead (ThermoFisher) for 10 minutes in PBS prior to staining for extracellular antigens in 1% FBS/2.5% HEPES/0.2% EDTA in PBS for 20 minutes at 4°C. For assessment of mitochondrial superoxide, cells were stained with 5uM MitoSOX Red (ThermoFisher) in PBS for 10 minutes at 37°C. Cells were then washed and fixed using IC fix kit (eBioscience). All antibodies were purchased from Biolegend. Data was acquired with Fortessa II and cell sorting on Aria III (BD Biosciences) and analysis was performed in Flowjo software, using FMO's for each antibody.

Adoptive transfer of FACS sorted Mo-AMs

Female WT or *Acod1*$^{-/-}$ mice were dosed with 0.05U bleomycin via the oropharyngeal route and lavaged at day 7 post bleomycin to obtain monocyte-recruited AMs (Mo-AMs). Cells recovered from bronchoaleolar lavage were stained with extracellular antibodies as described above and live, CD45^{+}, CD64^{+}, CD11c^{+}, SigF^{int} Mo-AMs were isolated by FACS sorting as shown in the gating strategy in **Supplementary Figure 2**. Subsequently, 50,000 WT or *Acod1*$^{-/-}$ Mo-AMs were administered via the oropharyngeal route to male *Acod1*$^{-/-}$ mice, which had been dosed with bleomycin 7 days prior . Mice were sacrificed at day 21 post initial bleomycin exposure.

Hydroxyproline assay

Hydroxyproline was measured using 10mg of tissue from the inferior lobe of murine samples using a Hydroxyproline Assay Kit (Sigma Aldrich), as per manufacturer's instructions and fold change of bleomycin/PBS groups was calculated.

Histology

Paraffin-embedded sections (4 µm) of lungs (apical lobe) were stained with hematoxylin/ eosin (H&E) and Sirius Red. For assessment of fibrosis, the semi-quantitative Ashcroft scoring system was used as previously described (Hübner et al., 2008). All scoring and measurements were performed by 3-5 blinded independent observers.

JULI-Stage Real-time cell recording

Primary human lung fibroblasts were seeded in 96-well plate for proliferation assay (5,000 per well) or 24-well plate for wound healing assay and serum-starved overnight prior to treatment with 10mM itaconate in complete DMEM for 48- 72 hrs. For wound healing assays, a standardised scratch was applied in each well using a p10 pipette tip. Images were taken in JULI-Stage system (NanoEntek) at three to five positions per well every 30 minutes and proliferation rate or wound closure were calculated using JULI-Stage software (NanoEntek).

Real-time PCR

Total RNA from the post-caval lobe was extracted using the QIAGEN RNeasy Mini Kit plus (QIAGEN) or using the QIAGEN RNeasy Micro Kit plus for total RNA from cell cultures and BAL cells. Total RNA was reverse transcribed into cDNA using the High Capacity cDNA Reverse Transcription kit (Life Technologies), or GoScript reverse transcription system (Promega) for AMs, according to manufacturer's instructions. Real-time PCR was performed using fast-qPCR mastermix (Life technologies) on a Viia-7 instrument (Applied Biosciences) with Taqman primers for murine *acod1, col-1α1, col3α1, col4α1, fn1, mmp2* or human *acod1, cd163, fn1, IL-1β, mmp1, mmp9* using *actb* (Life Technologies) as housekeeping gene. For analysis of murine AM fibrosis gene expression, total RNA (0.08 µg) of FACS sorted Mo-AMs or Tr-AMs was

reverse transcribed into cDNA using the RT^2 first-strand synthesis kit as per manufacturer's instructions (QIAGEN). Gene expression of 84 genes in murine fibrosis was assessed using fast-qPCR SYBR Green Master Mix (Qiagen, Germany) and mouse fibrosis 96-well genearray (120Z, QIAGEN) on a ViiA-7 instrument. Gene expression was analysed using the QIAGEN data analysis centre.

Seahorse analysis

FACS sorted murine Tr-/Mo-AM (100,000 per well) were plated in a Seahorse plate coated with Cell Tak (BD Biosciences) and analysed after resting at 37°C, 5% CO_2 overnight. Oxygen Consumption Rate (OCR) and extracellular acidification rate (ECAR) were measured in XF medium (nonbuffered RPMI containing 2mM glutamine, 1mM pyruvate and 10mM glucose, pH 7.4, Agilent) using the XFp extracellular flux analyser (Agilent). OCR and ECAR were measured under basal conditions and after the sequential addition of 1.5 µM Oligomycin, 2.0 µM FCCP and 0.5 µM Rotenone/Antimycin A (mito stress test, Agilent), which enabled the calculation of spare respiratory capacity from basal and maximal respiration as a result of OxPhos.

Quantification and Statistical Analysis

Differences between non-continuous groups were compared using the Mann-Whitney U test, one-way ANOVA with Sidak's multiple comparison test or a one-sample-t test where appropriate. Kaplan-Meier analysis was used to compare time to humane endpoint in mice. Data are presented as mean ±standard error of the mean (SEM). For *in vivo* experiments, the number of animals (n) per group are indicated. Analysis was performed using Prism software (GraphPad Software). PCA clustering was performed using the ClustVis package for R (available through Github, https://github.com/taunometsalu/ClustVis), (Metsalu et al., 2015). Heat-maps

were generated using Morpheus software tool (https://software.broadinstitute.org/morpheus/).

Supplementary information

Supplemental Table 1: Subject demographics of samples used for qPCR analysis (Figure 1A).

Table showing sex, age, drug-treatment, FEV1, FEV1 %predicted, forced vital capacity (FVC), % predicted FVC and smoking status of Healthy (n = 10) and IPF (n = 27) samples used for qPCR of ACOD1 (Figure 1A). Data presented as mean ± S.D.

	IPF (n = 27) (Mean ± S.D.)	Healthy (n = 10) (Mean ± S.D.)	T-Test
Sex (M/F)	21M/6F	5M/5F	
Age	69.5 ± 9.0	43.6 ± 11.0	****
On anti-fibrotic treatment **Of which:** **Nintednib** **Pifenidone**	41% 45% 55%	-	
On steroids	-	-	
FEV1	2.3 ± 0.7	2.8 ± 0.8	n.s.
FEV1 (predicted)	85.4 ± 18.5	NA	
FVC	2.8 ± 0.9	3.5 ±1.1	n.s.
FVC (predicted	81.8 ± 18.1	NA	
DLCO (single breath)	4.0 ± 1.7	NA	
Ever smoked **Of which:** **Ex-Smoker** **Current-smoker**	77% 90% 10%	20% 100%	

Supplemental Table 2: Subject demographics of samples used for GC-MS analysis (Figure 1B).

Table showing sex, age, drug-treatment, FEV1, FEV1 %predicted, forced vital capacity (FVC), % predicted FVC and smoking status of Healthy (n = 10) and IPF (n = 47) samples used for GC-MS of itaconate (Figure 1B). Data presented as mean ± S.D.

	IPF (n = 47) (Mean ± S.D.)	Healthy (n = 10) (Mean ± S.D.)	T-Test
Sex (M/F)	37/10	6/4	
Age	72.9 ± 7.7	46.6 ± 12.1	****
On anti-fibrotic treatment **Of which:** **Nintednib** **Pifenidone**	70% 36% 78%	-	
On steroids	8.5%	-	
FEV1	2.2 ± 0.6	3.0 ± 0.6	*
FEV1 (predicted)	84.6 ± 14.2	NA	
FVC	2.7 ± 0.8	3.7 ± 0.9	n.s.
FVC (predicted	80.6 ± 13.6	NA	
DLCO (single breath)	3.8 ± 1.4	NA	
Ever smoked **Of which:** **Ex-Smoker** **Current-smoker**	64% 87% 13%	33% - 100%	

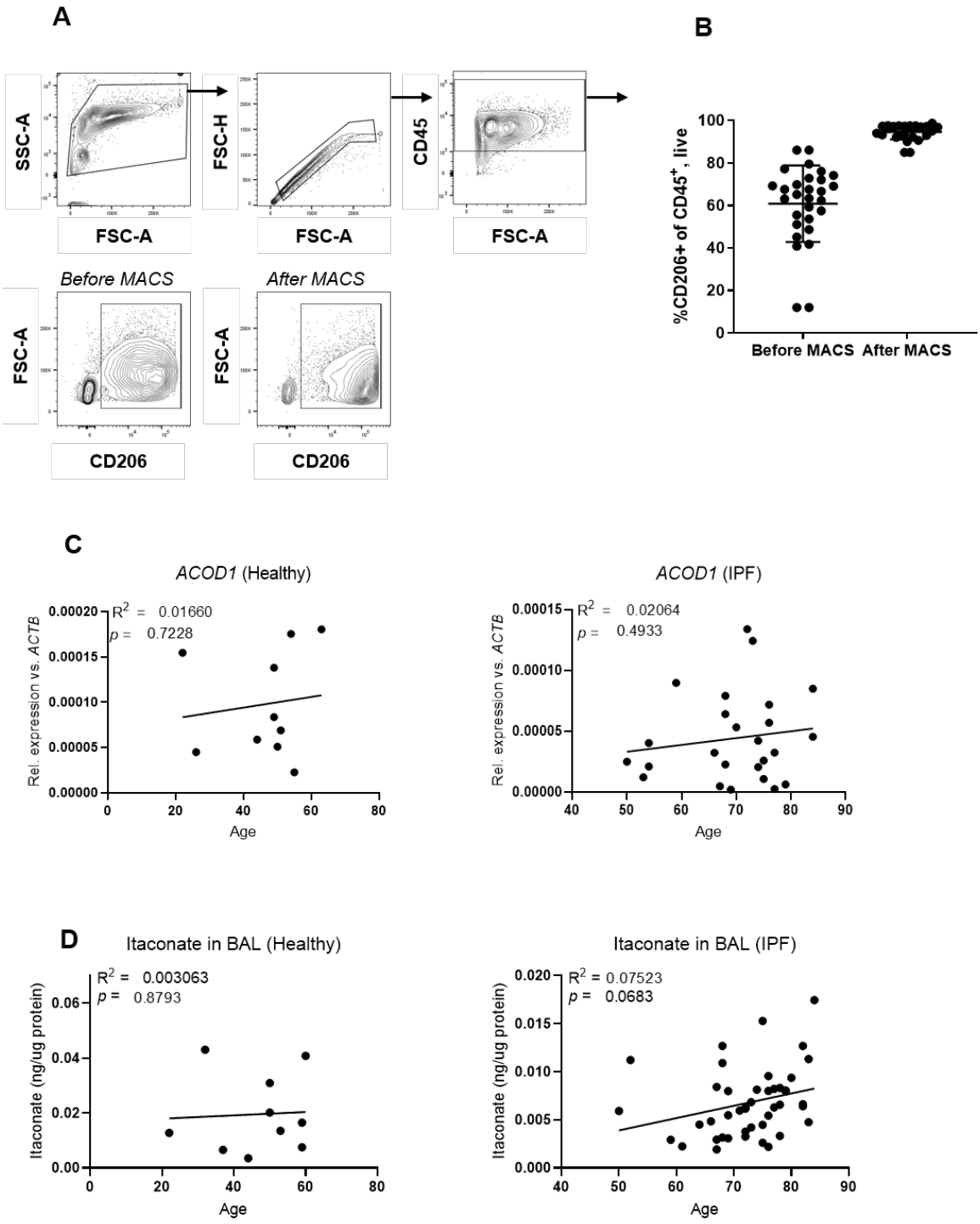

773

774 **Supplemental Figure 1: MACS sorting of human CD206$^+$ BAL AM**

775 (A) Representative FACS plots showing gating strategy to assess purity of human
776 CD45$^+$, CD206$^+$ BAL AM population before and after magnetic activated cell sorting
777 (MACS). (B) Purity of human CD45$^+$, CD206$^+$ BAL AM population confirmed by FACS,
778 before and after MACS (n = 29). (C) Linear regression analysis between relative gene

779 expression of *ACOD1* vs *ACTB* and age in healthy controls (n = 10) and IPF patients
780 (n = 27). (D) Linear regression analysis between itaconate measured in BAL
781 supernatant by targeted GC-MS, normalised to total protein (ng/μg protein) and age
782 in healthy controls (n = 10) and IPF patients (n = 47).

783 Data presented as mean ± S.D.

784
785

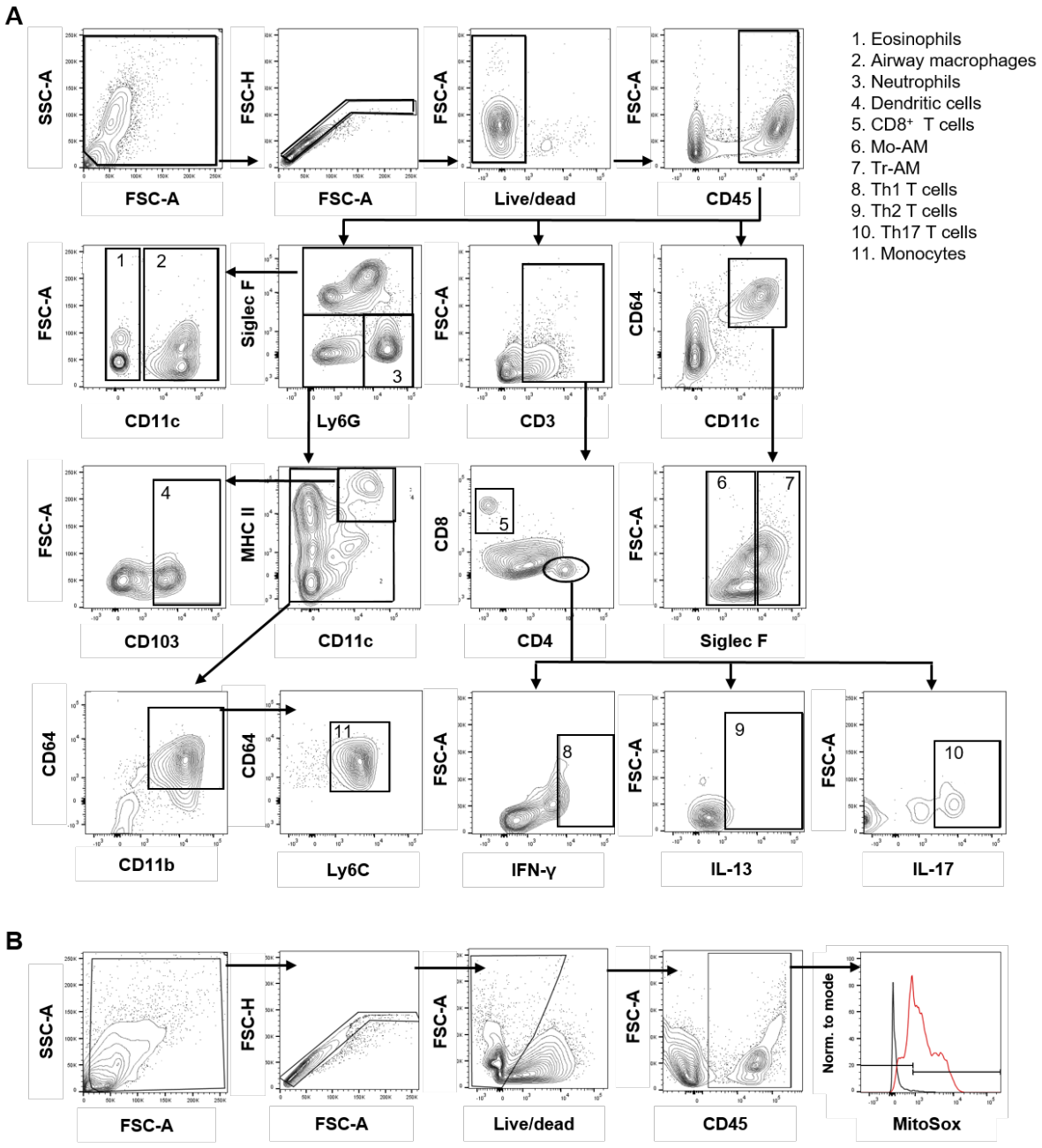

Supplemental Figure 2: Gating strategies of murine flow cytometry

(A) Representative FACS plots showing gating strategy to determine the following immune cell populations in murine BAL and lung: eosinophils, monocytes, airway macrophages (AM), including monocyte-recruited AMs (SigF^{int}), and tissue-resident AMs (SigF^{high}), , neutrophils, dendritic cells (DCs), T cells, including Th1-T-cells, Th2-T-cells and Th-17-T-cells. (B) Representative FACS plots showing gating strategy to determine expression of mitoSOX dye for superoxide in murine BAL CD45^{+} population.

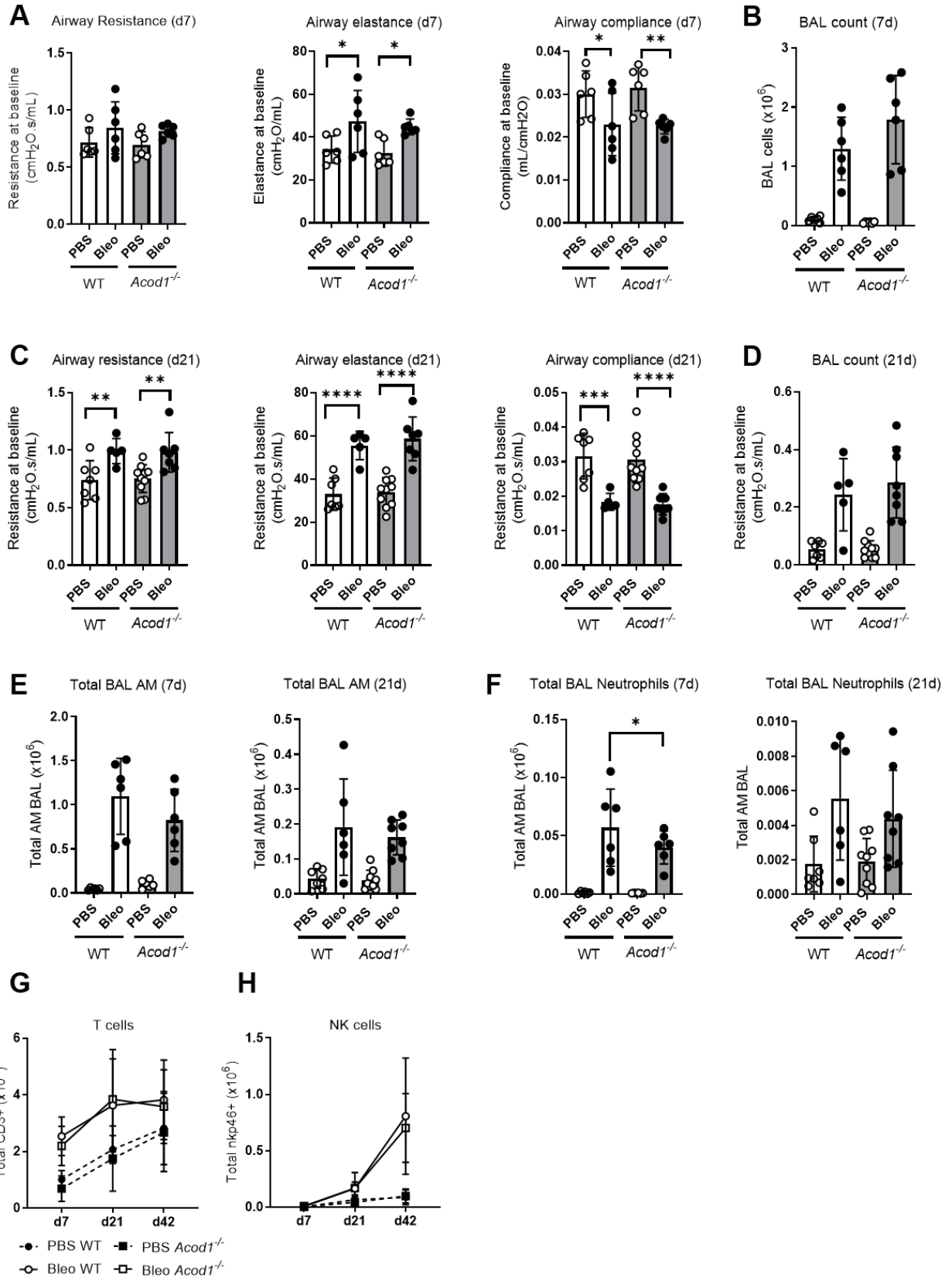
A
Airway Resistance (d7)
Resistance at baseline (cmH2O.s/mL)
Airway elastance (d7)
Elastance at baseline (cmH2O/mL)
Airway compliance (d7)
Compliance at baseline (mL/cmH2O)
B
BAL count (7d)
BAL cells (x10^6)
C
Airway resistance (d21)
Airway elastance (d21)
Airway compliance (d21)
D
BAL count (21d)
E
Total BAL AM (7d)
Total AM BAL (x10^6)
Total BAL AM (21d)
F
Total BAL Neutrophils (7d)
Total BAL Neutrophils (21d)
Total AM BAL
PBS
Bleo
WT
Acod1-/-
G
T cells
Total CD3+ (x10^6)
H
NK cells
Total nkp46+ (x10^6)
d7
d21
d42
PBS WT
PBS Acod1-/-
Bleo WT
Bleo Acod1-/-

Supplementary Figure 3: Lung function and immune cell profile after bleomycin treatment in Acod1$^{-/-}$ mice

(A) Resistance, elastance and compliance at baseline measured by FlexiVent in PBS and bleomycin dosed WT and *Acod1*$^{-/-}$ mice at day 7 post bleomycin (all groups n = 6). (B) Total BAL cells in PBS and bleomycin dosed WT and *Acod1*$^{-/-}$ mice at day 7 post bleomycin (all groups n = 6). (C) Resistance, elastance and compliance at baseline measured by FlexiVent in PBS and bleomycin dosed WT and *Acod1*$^{-/-}$ mice at day 21 post bleomycin; (n = 5 – 10, two experiments pooled). (D) Total BAL cells in PBS and bleomycin dosed WT and *Acod1*$^{-/-}$ mice at day 21 post bleomycin; (n = 5 – 10, two experiments pooled). (E) Total BAL AMs cells in PBS and bleomycin dosed WT and *Acod1*$^{-/-}$ mice at day 7 (n = 6 all groups) and day 21 (n = 5 -10) post bleomycin. (F) Total BAL neutrophils in PBS and bleomycin dosed WT and *Acod1*$^{-/-}$ mice at day 7 (n = 6 all groups) and day 21 (n = 5 -10) post bleomycin. (G - H) Total T-cells and NK-cells in BAL of PBS and bleomycin dosed WT and *Acod1*$^{-/-}$ mice at day 7, day 21 and day 42 (n = 3 – 6 per group) post bleomycin. Representative of two experiments. Data presented as mean ± S.D.; Significance was tested by One Way ANOVA + Sidak's multiple comparison test *$P < 0.05$, ** $P < 0.01$, *** $P < 0.001$.

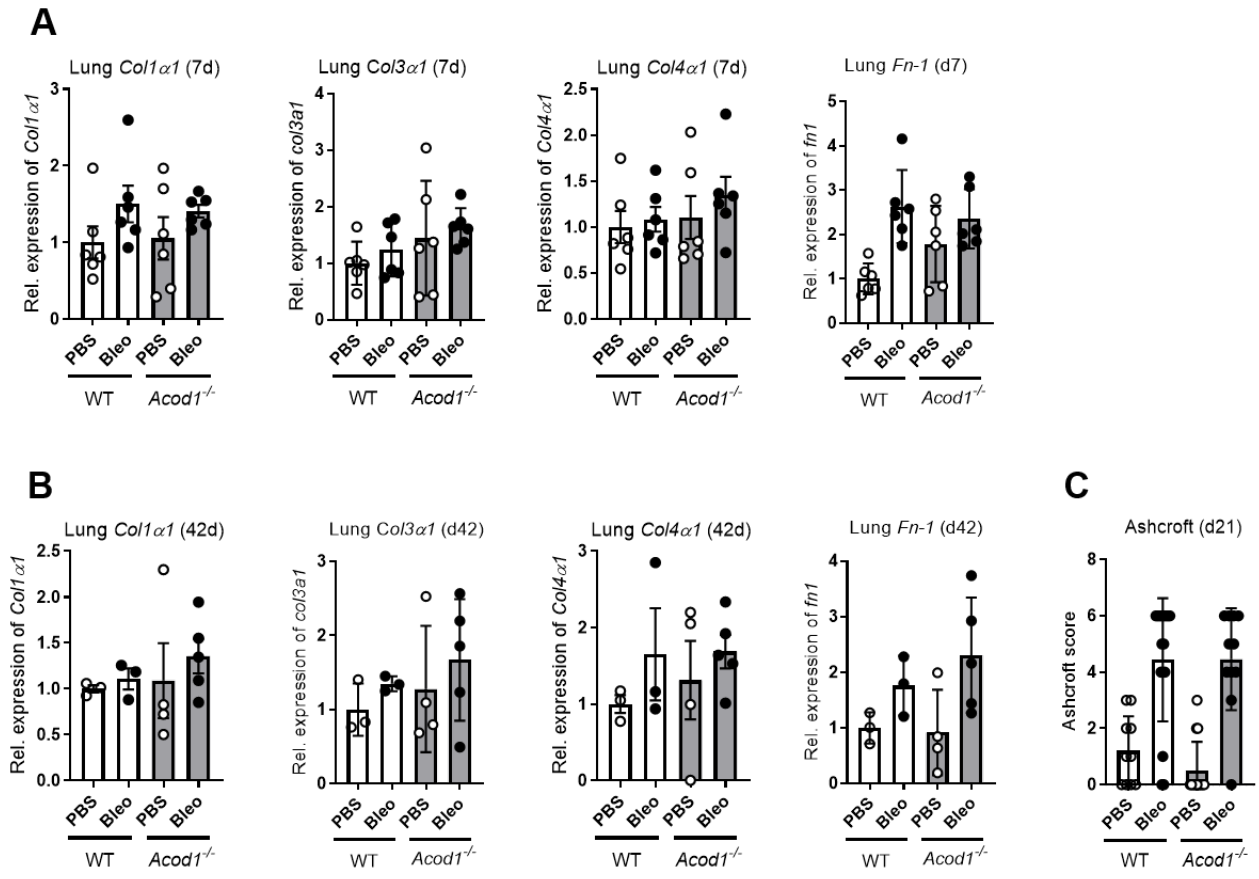

Supplementary Figure 4: Fibrotic phenotype in *Acod1*$^{-/-}$ mice at day 7 and day 21 post bleomycin

(A-B) Gene expression analysis of *Col1α1, Col3α1, Col4α1*, *Fn1* in lung homogenate of PBS and bleomycin dosed WT and *Acod1*$^{-/-}$ mice at day 7 (A) and day 42 (B) (n = 3-6). *Actb* was used as housekeeping gene. Pooled from two independent experiments. (C) Ashcroft score based on Sirius red staining in lung slices harvested at day 21 post bleomycin (n = 11 – 16 per group; three experiments pooled).

Data presented as mean ± S.D. Significance was tested by One Way ANOVA + Sidak's multiple comparison test.

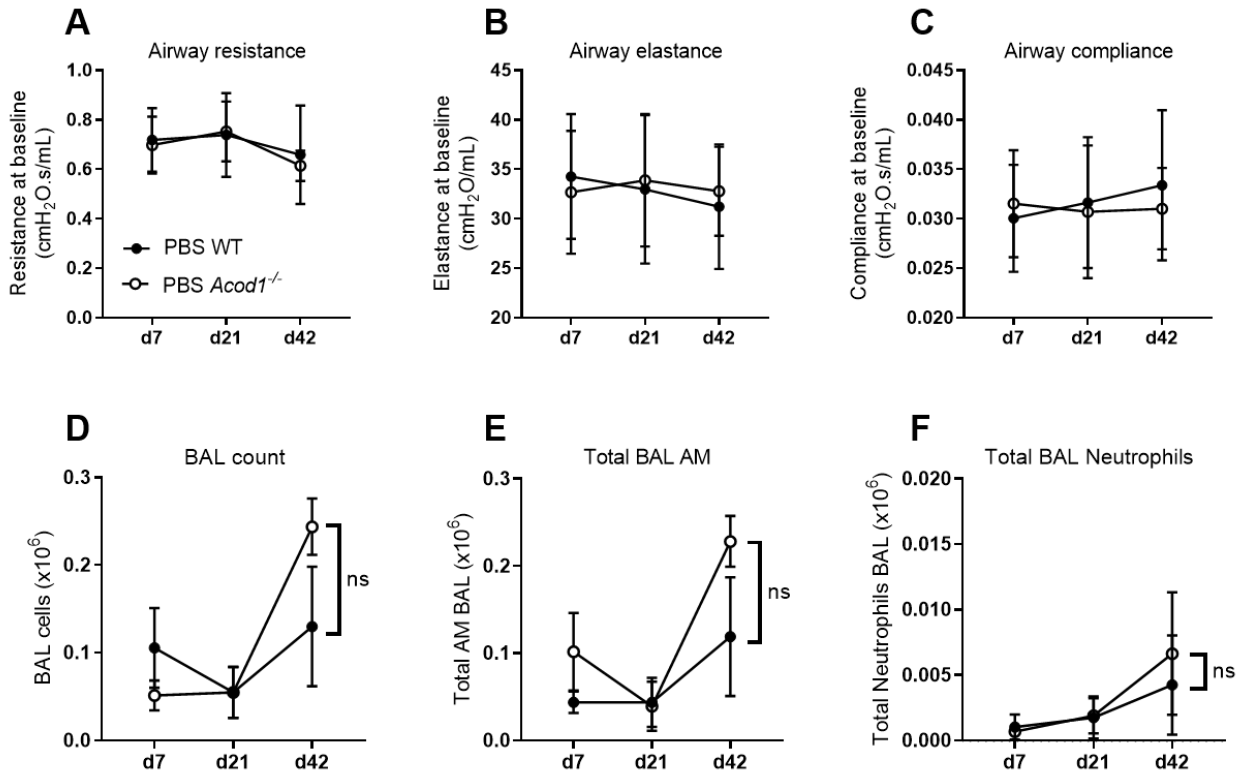

827

828 **Supplementary Figure 5: Baseline lung function and immune cell recruitment in**

829 **WT and *Acod1*$^{-/-}$ mice**

830 (A – C) Resistance (A), elastance (B) and compliance (C) at baseline measured by

831 FlexiVent in PBS dosed WT and *Acod1*$^{-/-}$ mice at day 7, day 21 and day 42. (D – F)

832 Total BAL cells (D), numbers of BAL AMs (E) and BAL neutrophils (F) in PBS dosed

833 WT and *Acod1*$^{-/-}$ mice at day 7, day 21 and day 42. Day 7 both groups n = 6, day 21

834 WT n = 7, Acod1-/- n = 10; day 42 WT n = 7, Acod1-/- n = 4; representative of 2 – 3

835 experiments per time point.

836

837 Data presented as mean ± S.D. Significance was tested by Mann-Whitney-U test per

838 time point.

839

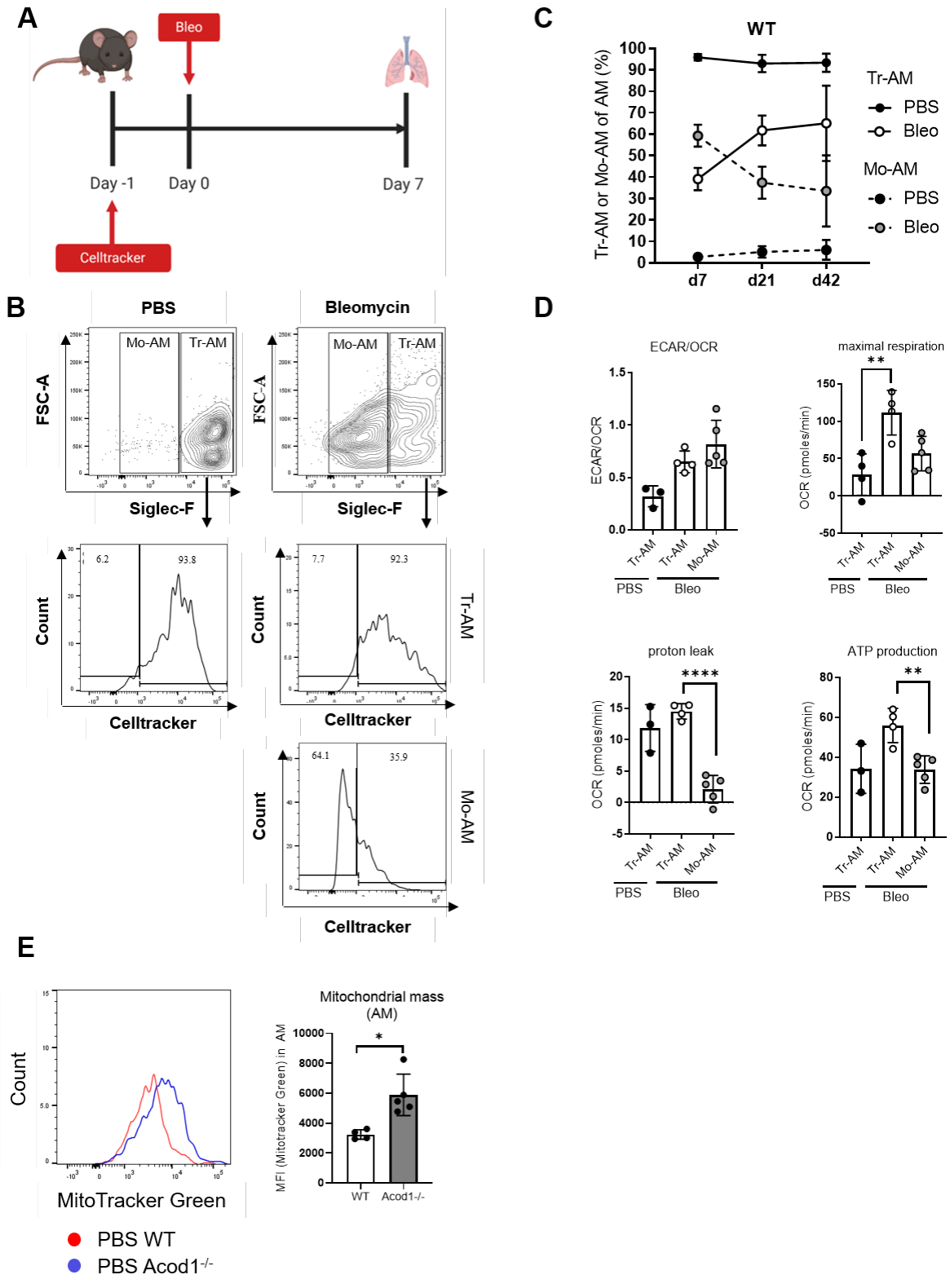

Supplementary Figure 6: Itaconate controls tissue resident AM metabolism

(A) Schematic of dosing regimen using 8-10 week old C57Bl/6 mice. 0.05U Bleomycin and 0.05µM PKH26 Celltracker was administered oropharyngeal at indicated time points. (B) Representative FACS plots showing gating strategy to assess PKH-26 Celltracker in Tr-AM and Mo-AM populations (see gating strategy in supplemental Fig. 2) in murine BAL after PBS or bleomycin treatment. (C) Tr-AM or Mo-AM as % of total AM in BAL of PBS or Bleomycin dosed WT mice at day 7, day 21 and day 42 post bleomycin exposure (n=6-12 per group). (D) Additional read-outs of seahorse mitochondrial stress test (Fig. 3A) of PBS Tr-AM (n=3), Bleo Tr-AM (n=4) and Bleo Mo-AM (n=5), representative of three independent experiments. (E) Representative graph of MitoTracker Green staining in WT and *Acod1*$^{-/-}$ PBS treated mice in the live, CD45^{+} fraction and quantification of mean fluorescent intensity (MFI) of WT (n=4) and *Acod1*$^{-/-}$ (n=5) PBS treated mice.

Data presented as mean ± S.D. Significance was tested by ordinary one-way ANOVA with Sidak's multiple comparison test (D) or Mann Whitney U test (F), ** $P < 0.01$, *** $P < 0.001$, ****$P < 0.0005$.

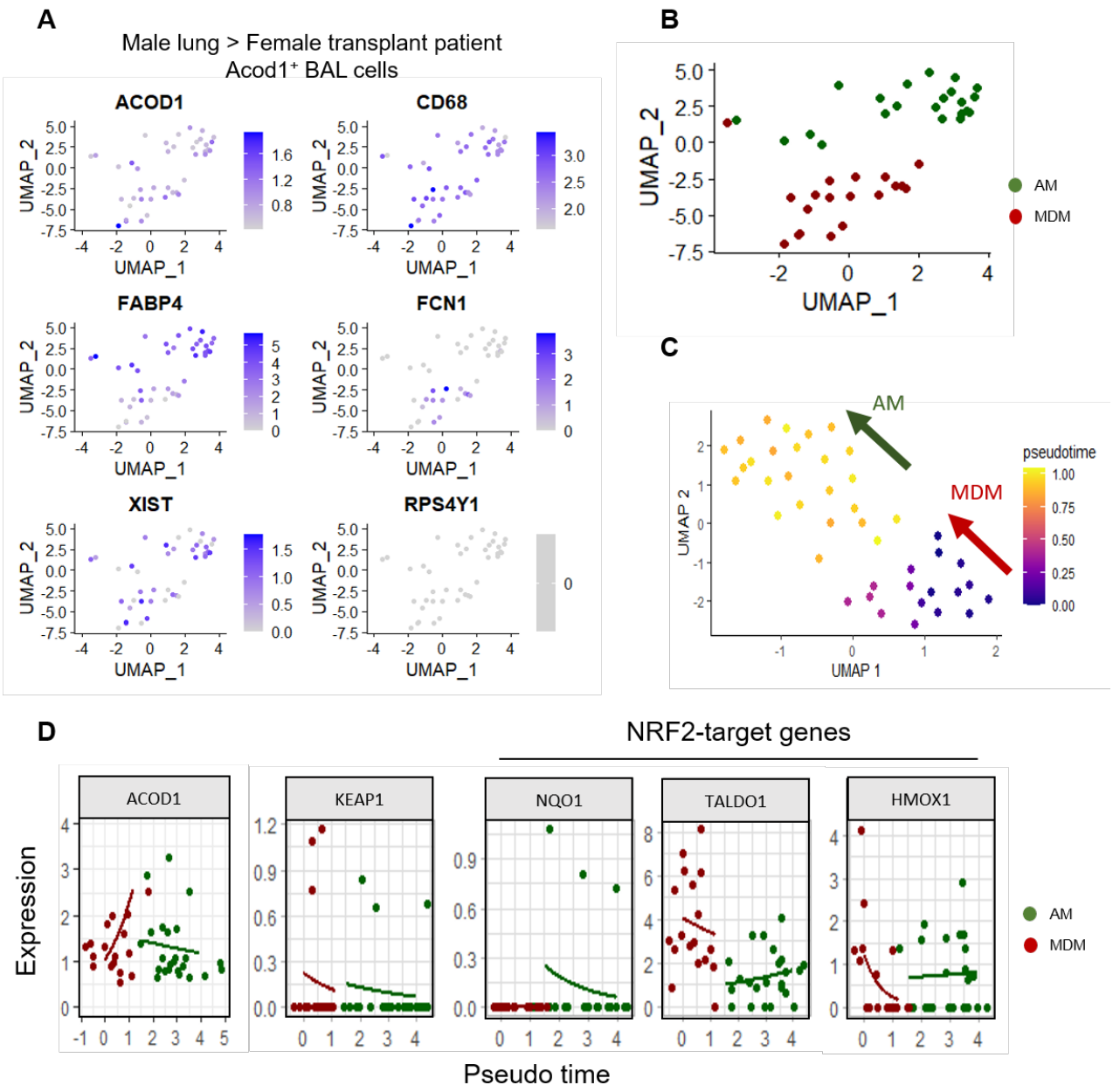

Supplemental Figure 7: AMs in the adult human lung after transplant express ACOD1. A) Acod1 expressing AM (CD68) in BAL after male donor (RPS4Y1) to female recipient (XIST) lung transplant. B) UMAP of Acod1 expressing AMs and monocyte derived macrophages (MDM). C) Pseudo time analysis of AM and MDM in BAL after male donor to female recipient lung transplant. D) Pseudo-time analysis of expression of *Acod1, KEAP1* and NRF2-target genes *NQO1, TALDO1* and *HMOX1* in AM and MDM after male donor to female recipient lung transplant.

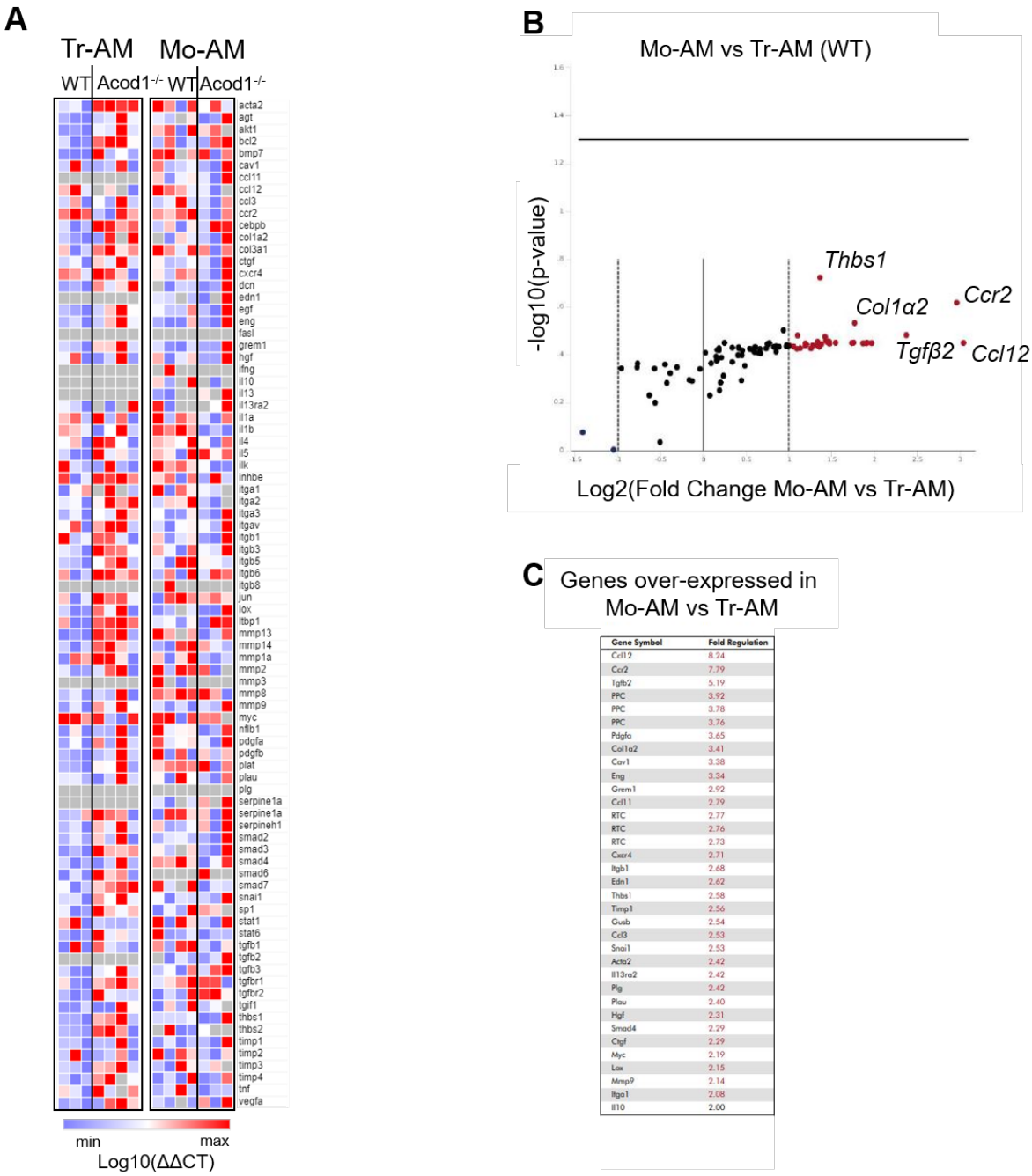

Supplementary Figure 8: Pro-fibrotic genes are increased in Mo-AM compared to Tr-AM after bleomycin exposure

(A) Heat map representation of murine fibrosis gene array of sorted Tr-AM and Mo-AM from WT and Acod1$^{-/-}$ 7 days post bleomycin exposure (n = 4 for all groups). Data shown as log10 of ΔΔCT WT vs Acod1$^{-/-}$ (B) Volcano plot highlighting differentially expressed genes in WT Mo-AM vs Tr-AM at day 7 post bleomycin exposure. Genes

up-regulated are shown in red and those down-regulated in blue. (C) Table highlighting fold change of fibrosis related genes of samples in (A).

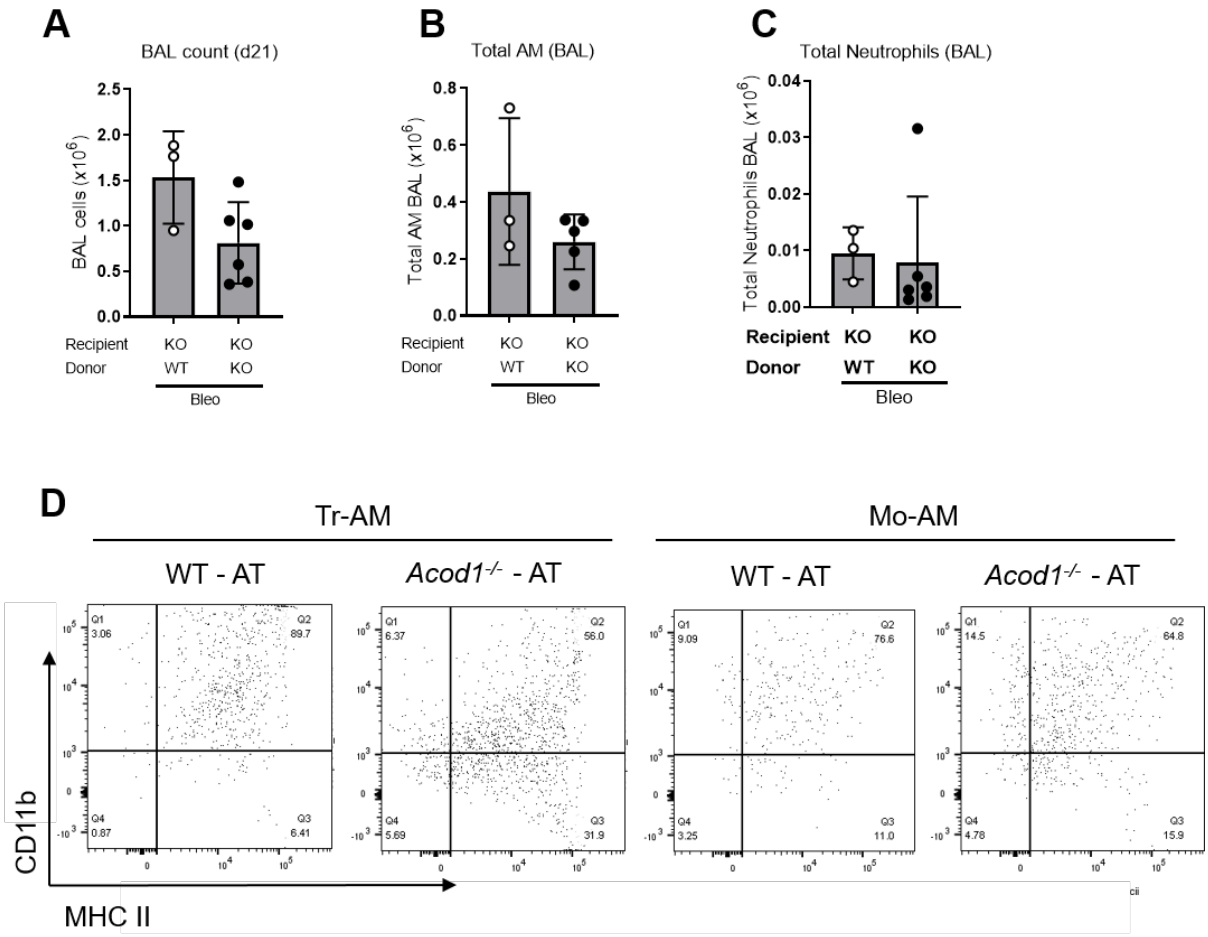

Supplementary Figure 9: BAL cell composition and collagen gene expression post adoptive transfer.

(A - C) Total BAL cells (A), numbers of BAL AMs (B) and BAL neutrophils (C) in PBS or Bleo dosed WT and *Acod1*$^{-/-}$ mice at day 42; WT-AT n = 3, KO-AT n = 6. (D) Representative FACS plots of CD11b^{+}/MHC II^{+} and CD11b^{-}/MHC II^{-} Tr-AM and Mo-AM in BAL of *Acod1*$^{-/-}$ mice after adoptive transfer of WT or *Acod1*$^{-/-}$ Mo-AMs; day 21 post bleomycin.

WT-AT = adoptive transfer of WT Mo-AMs into *Acod1*$^{-/-}$ mice, KO-AT = adoptive transfer of *Acod1*$^{-/-}$ Mo-AM into *Acod1*$^{-/-}$ mice. Data presented as mean ± S.D.; Significance was tested by Mann-Whitney U test.

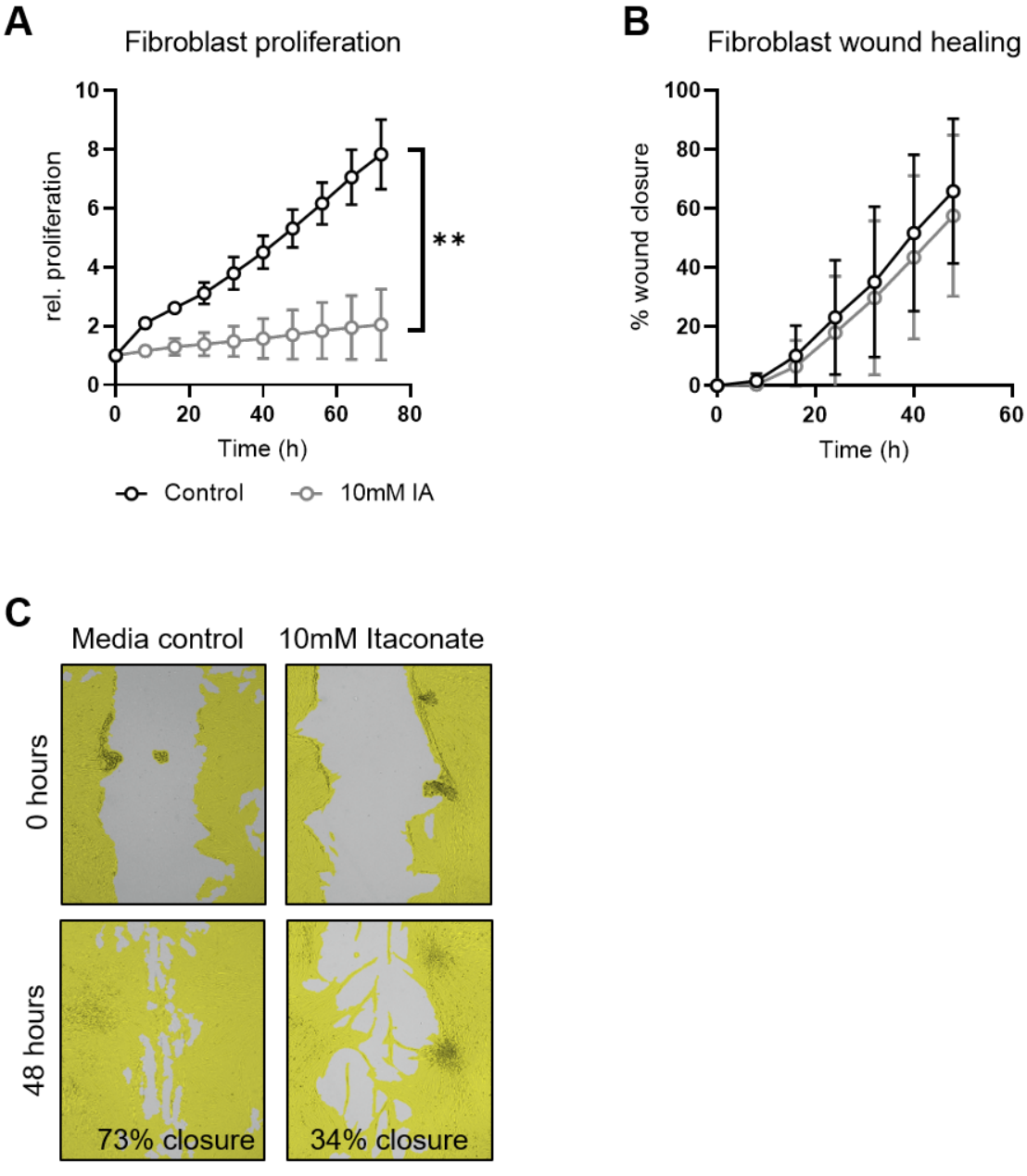

Supplementary Figure 10: Exogenous itaconate limits human lung fibroblast wound healing

(A) Proliferation rate of IPF (n = 3) human primary lung fibroblasts stimulated with 10mM itaconate or vehicle control measured using the JULI Stage system. (B) Wound healing capacity of healthy (n = 3) human primary lung fibroblasts stimulated with 10mM itaconate or vehicle control measured using the JuLI Stage system; (all groups n = 4). Two-tailed, unpaired t-test of area under the curve. (C) Representative images of fibroblast wound healing during stimulation with 10mM itaconate or vehicle control, acquired using the JULI stage system. Statistical significance tested by Mann-Whitney U test of area under the curve, ** $P < 0.01$.

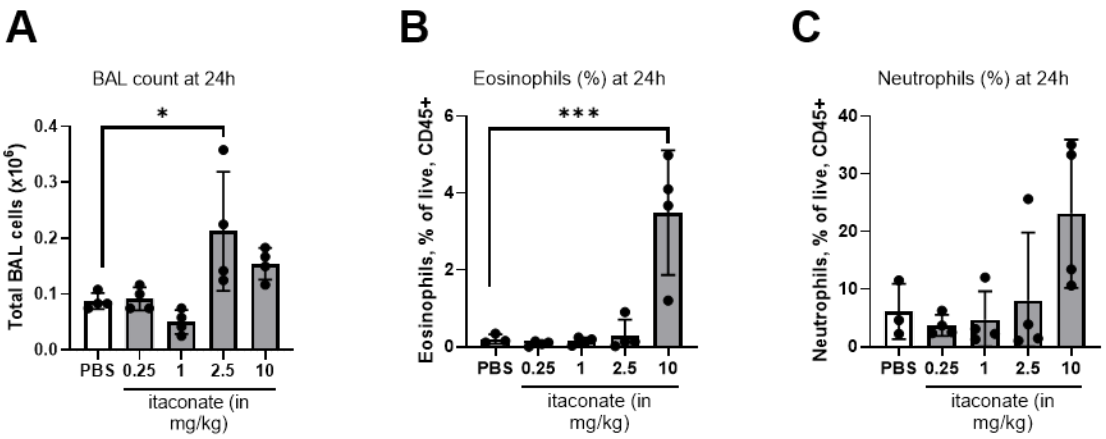

Supplementary Figure 11: Exogenous itaconate is anti-fibrotic

(A-C) Total BAL count, percentage of eosinophils (B) and Percentage of neutrophils (C) of PBS or itaconate dosed mice (0.25-10 mg/kg, oropharyngeal), 24h post administration (n = 4 per group).

Data presented as mean ± S.D..; Significance was tested by ordinary one-way ANOVA with Sidak's multiple comparison test, ** P < 0.01.

References

1. Allden, S.J., Ogger, P.P., Ghai, P., McErlean, P., Hewitt, R., Toshner, R., Walker, S.A., Saunders, P., Kingston, S., Molyneaux, P.L., et al. (2019). The Transferrin Receptor CD71 Delineates Functionally Distinct Airway Macrophage Subsets during Idiopathic Pulmonary Fibrosis. Am. J. Respir. Crit. Care Med. *200, 209-219*.

2. Atabai, K., Jame, S., Azhar, N., Kuo, A., Lam, M., McKleroy, W., DeHart, G., Rahman, S., Xia, D.D., Melton, A.C., et al. (2009). Mfge8 diminishes the severity of tissue fibrosis in mice by binding and targeting collagen for uptake by macrophages. J. Clin. Invest. *119*, 3713–3722.

3. Basler, T., Jeckstadt, S., Valentin-Weigand, P., and Goethe, R. (2006). Mycobacterium paratuberculosis, Mycobacterium smegmatis and lipopolysaccharide induce different transcriptional and post-transcriptional regulation of the IRG1 gene in murine macrophages . J. Leukoc. Biol. *79*, 628–638.

4. Bharat, A., Bhorade, S. M., Morales-Nebreda, L., McQuattie-Pimentel, A. C., Soberanes, S., Ridge, K. et al. (2016). Flow cytometry reveals similarities between lung macrophages in humans and mice. Am J Respir Crit Care Med *54*(1), 147-149.

5. Byrne, A. J., Powell, J. E., O'Sullivan, B. J., Ogger, P. P., Hoffland, A., Cook, J. et al. (2020). Dynamics of human monocytes and airway macrophages during healthy aging and after transplant. The Journal of Experimental Medicine, 217(3).

6. Byrne, A.J., Mathie, S.A., Gregory, L.G., and Lloyd, C.M. (2015). Pulmonary

933 macrophages: key players in the innate defence of the airways. Thorax *70*,
934 1189–1196.

935 7. Byrne, A.J., Maher, T.M., and Lloyd, C.M. (2016). Pulmonary Macrophages: A
936 New Therapeutic Pathway in Fibrosing Lung Disease? Trends Mol. Med. *22*,
937 303–316.

938 8. Byrne, A.J., Weiss, M., Mathie, S.A., Walker, S.A., Eames, H.L., Saliba, D.,
939 Lloyd, C.M., and Udalova, I.A. (2017). A critical role for IRF5 in regulating
940 allergic airway inflammation. Mucosal Immunol. *10*, 716–726.

941 9. Cordes, T., Wallace, M., Michelucci, A., Divakaruni, A.S., Sapcariu, S.C.,
942 Sousa, C., Koseki, H., Cabrales, P., Murphy, A.N., Hiller, K., et al. (2016).
943 Immunoresponsive gene 1 and itaconate inhibit succinate dehydrogenase to
944 modulate intracellular succinate levels. J. Biol. Chem. *291*, 14274–14284.

945 10. Dancer, R.C.A., Wood, A.M., and Thickett, D.R. (2011). Metalloproteinases in
946 idiopathic pulmonary fibrosis. Eur. Respir. J. *38*, 1461–1467.

947 11. Domínguez-Andrés, J., Novakovic, B., Li, Y., Scicluna, B.P., Gresnigt, M.S.,
948 Arts, R.J.W., Oosting, M., Moorlag, S.J.C.F.M., Groh, L.A., Zwaag, J., et al.
949 (2019). The Itaconate Pathway Is a Central Regulatory Node Linking Innate
950 Immune Tolerance and Trained Immunity. Cell Metab. *29*, 211–220.e5.

951 12. Hübner, R.H., Gitter, W., El Mokhtari, N.E., Mathiak, M., Both, M., Bolte, H.,
952 Freitag-Wolf, S., and Bewig, B. (2008). Standardized quantification of
953 pulmonary fibrosis in histological samples. Biotechniques *44*, 507–517.

954 13. Hussell, T., and Bell, T.J. (2014). Alveolar macrophages: plasticity in a tissue-
955 specific context. Nat. Rev. Immunol. *14*, 81–93.

14. Hutchinson, J., Fogarty, A., Hubbard, R., and McKeever, T. (2015). Global incidence and mortality of idiopathic pulmonary fibrosis: A systematic review. Eur. Respir. J. *46*, 795–806.

15. Jenkins, R.G., Moore, B.B., Chambers, R.C., Eickelberg, O., Melanie, K., Kolb, M., Laurent, G.J., Nanthakumar, C.B., Olman, M.A., Pardo, A., et al. (2017). An Of fi cial American Thoracic Society Workshop Report : Use of Animal Models for the Preclinical Assessment of Potential Therapies for Pulmonary Fibrosis. *56*, 667–679.

16. Kendall, R.T., and Feghali-Bostwick, C.A. (2014). Fibroblasts in fibrosis: Novel roles and mediators. Front. Pharmacol. *5 MAY*, 1–13.

17. Kreuter, M., Bonella, F., Wijsenbeek, M., Maher, T.M., and Spagnolo, P. (2015). Pharmacological Treatment of Idiopathic Pulmonary Fibrosis: Current Approaches, Unsolved Issues, and Future Perspectives. Biomed Res. Int. *2015*.

18. Lampropoulou, V., Sergushichev, A., Bambouskova, M., Nair, S., Vincent, E.E., Loginicheva, E., Cervantes-Barragan, L., Ma, X., Huang, S.C.-C., Griss, T., et al. (2016). Itaconate Links Inhibition of Succinate Dehydrogenase with Macrophage Metabolic Remodeling and Regulation of Inflammation. Cell Metab. *24*, 158–166.

19. Lee, C.G.L., Jenkins, N.A., Gilbert, D.J., Copeland, N.G., and O'Brien, W.E. (1995). Cloning and analysis of gene regulation of a novel LPS-inducible cDNA. Immunogenetics.

20. Martinez, F.J., Collard, H.R., Pardo, A., Raghu, G., Richeldi, L., Selman, M., Swigris, J.J., Taniguchi, H., and Wells, A.U. (2017). Idiopathic pulmonary

fibrosis. Nat. Rev. Dis. Prim. *3*.

21. Meiser, J., Kraemer, L., Jaeger, C., Madry, H., Link, A., Lepper, P.M., Hiller, K., and Schneider, J.G. (2018). Itaconic acid indicates cellular but not systemic immune system activation. Oncotarget *9*, 32098–32107.

22. Metsalu, T., Vilo, J., Science, C., and Liivi, J. (2015). ClustVis : a web tool for visualizing clustering of multivariate data using Principal Component Analysis and heatmap. *43*, 566–570.

23. Michelucci, A., Cordes, T., Ghelfi, J., Pailot, A., Reiling, N., Goldmann, O., Binz, T., Wegner, A., Tallam, A., Rausell, A., et al. (2013). Immune-responsive gene 1 protein links metabolism to immunity by catalyzing itaconic acid production. Proc. Natl. Acad. Sci. *110*, 7820–7825.

24. Mills, E.L., Kelly, B., Logan, A., Costa, A.S.H., Varma, M., Bryant, C.E., Tourlomousis, P., Däbritz, J.H.M., Gottlieb, E., Latorre, I., et al. (2016). Succinate Dehydrogenase Supports Metabolic Repurposing of Mitochondria to Drive Inflammatory Macrophages. Cell 457–470.

25. Mills, E.L., Ryan, D.G., Prag, H.A., Dikovskaya, D., Menon, D., Zaslona, Z., Jedrychowski, M.P., Costa, A.S.H., Higgins, M., Hams, E., et al. (2018). Itaconate is an anti-inflammatory metabolite that activates Nrf2 via alkylation of KEAP1. Nature *556*, 113–117.

26. Misharin, A. V., Morales-Nebreda, L., Reyfman, P.A., Cuda, C.M., Walter, J.M., McQuattie-Pimentel, A.C., Chen, C.-I., Anekalla, K.R., Joshi, N., Williams, K.J.N., et al. (2017). Monocyte-derived alveolar macrophages drive lung fibrosis and persist in the lung over the life span. J. Exp. Med. *214*, 2387–2404.

27. Moeller, A., Ask, K., Warburton, D., Gauldie, J., & Kolb, M. (2008). The bleomycin animal model: a useful tool to investigate treatment options for idiopathic pulmonary fibrosis? Int J Biochem Cell Biol *40*(3), 362-382.

28. Moore, B.B., and Hogaboam, C.M. (2008). Murine models of pulmonary fibrosis. Am. J. Physiol. - Lung Cell. Mol. Physiol. *294*, 152–160.

29. Murray, P.J., Allen, J.E., Biswas, S.K., Fisher, E.A., Gilroy, D.W., Goerdt, S., Gordon, S., Hamilton, J.A., Ivashkiv, L.B., Lawrence, T., et al. (2014). Macrophage activation and polarization: nomenclature and experimental guidelines. Immunity *41*, 14–20.

30. Nair, S., Huynh, J.P., Lampropoulou, V., Loginicheva, E., Esaulova, E., Gounder, A.P., Boon, A.C.M., Schwarzkopf, E.A., Bradstreet, T.R., Edelson, B.T., et al. (2018). Irg1 expression in myeloid cells prevents immunopathology during M. tuberculosis infection . J. Exp. Med. *215*, 1035–1045.

31. O'Neill, L.A.J., Kishton, R.J., and Rathmell, J. (2016). A guide to immunometabolism for immunologists. Nat. Rev. Immunol. *16*, 553–565.

32. Redente, E.F., Jacobsen, K.M., Solomon, J.J., Lara, A.R., Faubel, S., Keith, R.C., Henson, P.M., Downey, G.P., and Riches, D.W.H. (2011). Age and sex dimorphisms contribute to the severity of bleomycin-induced lung injury and fibrosis. Am. J. Physiol. Cell. Mol. Physiol. *301*, L510–L518.

33. Ren, K., Lv, Y., Zhuo, Y., Chen, C., Shi, H., Guo, L., Yang, G., Hou, Y., and Tan, X. (2016). Suppression of IRG-1 Reduces Inflammatory Cell Infiltration and Lung Injury in Respiratory Syncytial Virus Infection by Reducing. *90*, 7313–7322.

34. Schafer, M.J., White, T.A., Iijima, K., Haak, A.J., Ligresti, G., Atkinson, E.J., Oberg, A.L., Birch, J., Salmonowicz, H., Zhu, Y., et al. (2017). Cellular senescence mediates fibrotic pulmonary disease. Nat. Commun. *8*.

35. Shin, J.H., Yang, J.Y., Jeon, B.Y., Yoon, Y.J., Cho, S.N., Kang, Y.H., Ryu, D.H., and Hwang, G.S. (2011). 1H NMR-based metabolomic profiling in mice infected with Mycobacterium tuberculosis. J. Proteome Res. *10*, 2238–2247.

36. Strelko, C.L., Lu, W., Dufort, F.J., Seyfried, T.N., Chiles, T.C., Rabinowitz, J.D., and Roberts, M.F. (2011). Itaconic acid is a mammalian metabolite induced during macrophage activation. J. Am. Chem. Soc. *133*, 16386–16389.

37. Wynn, T.A., and Vannella, K.M. (2016). Macrophages in Tissue Repair, Regeneration, and Fibrosis. Immunity *44*, 450–462.

Acknowledgments:

PPO is supported by a National Heart and Lung Foundation studentship and a Studienstiftung des Deutschen Volkes fellowship. AJB is supported by a Joan Bending, Evelyn Bending, Mervyn Stephens + Olive Stephens Memorial Fellowship (AUK-SNF-2017-381) and a Wellcome Trust Seed award (205949/Z/17/Z). PLM is supported by an Action for Pulmonary Fibrosis Mike Bray fellowship. TMM is supported by an NIHR Clinician Scientist Fellowship (NIHR ref: CS-2013-13-017) and a British Lung Foundation Chair in Respiratory Research (C17-3). CML is a Wellcome Senior Fellow in Basic Biomedical Science (107059/Z/15/Z). The authors acknowledge the support of the flow cytometry facility at the South-Kensington campus and in particular Ms. Jane Srivastava, Dr. Jessica Rowley and Ms. Radhika Patel. We further thank Lorraine Lawrence at the Imperial College Histology Facility

for paraffin embedding, sectioning and staining of fixed lung tissue. Schematics and graphical abstract were created with BioRender (Biorender.com). We also thank Prof. Ann O'Gara (Imperial College London, U.K. and the Francis Crick Institute, U.K.) for critically reading of this manuscript and for providing invaluable feedback.

Author Contributions:

PPO, CML, TMM and AJB designed the study; PPO, GA, PG, SAW, PMcE, RH, BJO'S, JEP, EC, PS, SK, DCC, PLM and AJB carried out the work. RH, PLM, TMM consented patients and carried out bronchoscopies. All authors were involved in the interpretation of the results and in drafting and/or revising the manuscript, provided final approval, and vouch for the content of the final manuscript.

Declaration of interests

Unrelated to the current work, TMM has, via his institution, received industry-academic funding from GlaxoSmithKline R&D and UCB and has received consultancy or speakers fees from Apellis, Astra Zeneca, Bayer, Blade Therapeutics, Boehringer Ingelheim, Bristol-Myers Squibb, Galapagos, GlaxoSmithKline R&D, Indalo, Novartis, Pliant, ProMetic, Respivnat, Roche, Samumed and UCB. PLM received, unrelated to the submitted work, speaker and advisory board fees from Boehringer Ingelheim and Hoffmann-La Roche, via his institution. The authors declare no further conflicts of interest.